TEMPERATURE, CHOLESTEROL & THE MITOCHONDRIAL OUTER MEMBRANE

THE EFFECT OF CHOLESTEROL ON THE STRUCTURE OF MITOCHONDRIAL LIKE LIPID BILAYERS: AN X-RAY STUDY

By AMIT PATEL, M.Sc.

A Thesis Submitted to the School of Graduate Studies in Partial Fulfilment of the Requirements for the Degree Master of Science

Descriptive Note

Mcmaster University MASTER OF SCIENCE (2013) Hamilton, Ontario

Title: A Supported Bilayer Model to Study the Bcl-2 Family of Proteins and Their Interactions With the Mitochondrial Outer Membrane AUTHOR: Amit Patel, M.Sc. (McMaster University) SUPERVISOR: Professor Dr. Cecile Fradin NUMBER OF PAGES: ix, 67

Abstract:

Apoptosis plays a key role in the regulation and development of healthy multicellular organisms throughout their lifetimes. The mitochondria play a key role in this cellular process, as it contains proapoptotic factors, which once released into the cytosol of the cell, results in the death of the cell. The Bcl-2 family of proteins play a key role in apoptosis, acting as the gateway between life and death of the cell. Proteins such as tBid and Bax act to permeabilize the mitochondrial outer membrane (MOM), releasing the proapoptotic factors into the cell's cytosol. The interactions between these proteins and the mitochondrial outer membrane have yet to be fully understood. The lipid composition and cholesterol content of the membrane effectively inhibit or promote pore formation by Bax. Specifically, the addition of cholesterol into the membrane inhibits pore formation. This thesis attempts to further understand the effects cholesterol has on the structure of the MOM, and link those changes to the inhibited activity of Bax pore formation. MOM-like lipid bilayers were studied under varying temperatures and with the addition of cholesterol using x-ray reflectivity. Increasing temperatures from 10°C to 30°C resulted in bilayer thinning, as did decreasing cholesterol concentrations below 30%. From 10°C to 20°C, bilayer thickness showed a bell shaped profile, and changed to a linear decrease above about 20°C. This may assist Bax in pore formation, as it has also been observed to cause bilayer thinning. Increasing Cholesterol concentrations up to 30% resulted in little variation in bilayer thickness though hindrance of Bax pore formation is observed at content levels as low as 8%. Thus it is unlikely that bilayer thickening by cholesterol

causes the inhibition of Bax pore formation. In addition, cholesterol was observed to increase the electron density of the core of the bilayer at concentration levels above 25%.

Acknowledgements

First and foremost, I would like to thank my supervisor Dr. Cecile Fradin for all of her help and guidance throughout the course of my Masters, making sure I had a clear direction in my research at all times.

In addition, I would also like to thank Dr. Maikel Rheinstädter for the use of his lab as well as his continual assistance throughout my Masters, including sample preparation, data collection and analysis.

I would also like to thank Dr. Kari Dalnoki-Veress for helping guide me through my project, and defining clear and achievable milestones.

Finally, I would like to thank Dr. Norbert Kučerka for assisting with the data analysis process and its minute details.

Table of Contents

Descriptive Note ii
Abstract: iii
Acknowledgements v
Table of Contents vi
List of Figures and Tables: viii
List of Abbreviations and Symbols ix
Declaration of Academic Achievement xi
Introduction: 1
1) Biological Background 1
1. 1) Biological Importance of Cell Death 1
1.2) Variety in Cellular Death Pathways 2
1.3) Apoptotic Pathways 3
1.3.1) Bcl-2 Family Proteins Pathway Overview 4
1.3.2) Bcl-2 Family Protein Structures 6
1.3.3) Bid: Structure and Function 8
1.3.4) Bax: Structure and Function 8
1.4) Lipids and Pore Formation 9
1.5) Mitochondial Outer Membrane 11
1.6) Cholesterol and Membranes 15
1.7) Bcl-2 Family Proteins, Lipids, and Cholesterol Interactions 16
1.8)Model System: Solid Supported Lipid Bilayers 18
Materials & Methods: 20
2) Materials 20
2.1) Solid Support: Silicon 20
2.2) Chemicals & Salts 20
2.3) Lipids and Cholesterol 21
3) Methods 24

3.1) Lipid & Cholesterol Solution Preparation 24
3.2) Silicon Substrate Preparation 25
3.3) Sample Preparation: Lipid Deposition 27
3.4) Quartz Sample Protocol Adjustments 29
3.5) X-ray Reflectivity 29
3.5.1) Instrument: B.L.A.D.E. 29
3.5.2) Reflectivity Measurements 31
3.5.3) Data Analysis: Theory 33
3.5.4) Data Analysis Software 36
Results & Discussion: 38
4) Sample Preparation Refinement 38
4.1) Experimental Procedures Quality Check 41
4.2) APTES Quality Check 43
4.3) Deposition Temperature Quality Check 45
4.4) Substrate Effects on Multilayer Formation 47
5) Data Analysis: Phase Determination 51
6) Temperature Effects on Membrane Structure 53
7) Cholesterol Effects on Membrane Structure 59
7.1) Cholesterol & Membrane Homogeneity 59
7.2) Cholesterol and Membrane Structure 62
Conclusion: 66
References 69

List of Figures and Tables:

Title	Page
Figure 1: Structural Differences Between Apoptosis & Necrosis.	3
Figure 2: Artistic Rendition of Mitochondria.	4
Figure 3: Bcl-2 Homology (BH) Regions	7
Table 1: Examples of Bcl-2 Proteins.	7
Figure 4: Artistic Rendition of Pore Types.	11
Table 2: Lipid and Cholesterol Structures and Distributions.	14
Figure 5: Cholesterol Effects on Bax Pore Formation.	18
Table 3: Relative Humidity Induced by Salts.	21
Table 4: Lipid Properties.	24
Figure 6: APTES Layer on Silicon Wafer.	27
Figure 7: Experimental Setup and Geometry.	31
Figure 8: Fresnel Reflectivity Profile.	33
Figure 9: Standard Sample Preparation Protocol Effects on MOM-Like Samples.	39
Table 5: Standard Sample Preparation Protocol.	40
Figure 10: Experimental Technique Comparison.	43
Figure 11: Sample Quality Dependence on Acid Bath (AB) Temperature.	45
Figure 12: Sample Quality Dependence on Deposition Temperature.	47
Figure 13: Substrate Effects on Sample Quality.	49
Table 6: Modified Sample Preparation Protocol.	50
Figure 14: MOM-Like SSLB Data Analysis Outline.	52
Figure 15: Temperature Effects on MOM-Like Bilayers.	55
Figure 16: Temperature Related Changes to MOM-Like Samples.	58
Figure 17: Cholesterol X-Ray Reflectivity Profiles.	60
Figure 18: Continuous Transforms for Cholesterol Samples.	61
Figure 19: Cholesterol Electron Density Profiles.	63
Figure 20: Cholesterol Effects on MOM.	64

List of Abbreviations and Symbols

Abbreviation	Expansion
v_n	n^{th} order phase
2θ-scan	Specular Reflectivity Scan
Å	Angstrom
AB	Acid Bath
APTES	(3-Aminopropyl)triethoxysilane
B.L.A.D.E.	Biological Large Angle Diffraction Experiments
BD	3 Dimensional Rocker (Belly Dancer)
BH	Bcl-2 Homology
cBid	Cleaved-Bid
CL	Cardiolipin
cm	Centimeter
d	Bilayer + Water Layer Thickness
DMPC	1,2-dimyristoyl-sn-glycero-3-phosphocholine
dp-p	Bilayer Thickness (peak-to-peak distance)
dw	Water Layer Thickness
d_z	Unit Cell Length
ED	Electron Density
ETM	Embedded Together Model
$F(q_z)$	Form Factor
H_2O_2	Hydrogen Peroxide
H_2SO_4	Sulfuric Acid
ILL	Institut Laue-Langevin
IMS	Intermembrane Space
I_n	Integrated Intensity of n^{th} Order Peak
K_2SO_4	Potassium Sulphate
KCl	Potassium Chloride
k_f	Reflected Wave Vector
k_i	Incident Wave Vector
KNO_3	Potassium Nitrate
MIM	Mitochondrial Inner Membrane
MOM	Mitochondrial Outer Membrane
MOMP	Mitochondrial Outer Membrane Permiabilization
NaCl	Sodium Chloride
PC	Phosphatidylcholine
PE	Phosphatidylethanolamine
PI	Phosphatidylinositol
PS	Phosphatidylserine

Abbreviation	**Expansion**
q_c	Critical Angle in q Notation
q_z	Momentum Transfer Vector
$R(q_z)$	Reflected Intensity
RT	Room Temperature
$S(q_z)$	Structure Factor
SSLB	Solid Supported Lipid Bilayer
$T(q_z)$	Continuous Transform
tBid	Truncated-Bid
αH	Alpha Helice
Δdp-p	Change in Bilayer Thickness
Δdw	Change in Water Layer Thickness
θ	Incident/Reflected Angle
θ_c	Critical Angle
λ	Wavelength
π	Pi
ρ	Electron Density
ρ_W	Electron Density of Water

Declaration of Academic Achievement

ANTS/DPX fluorescence graph (Figure 5) was kindly provided by Aisha Shamas-Din.

Matt Barrett provided data for a standard reflectivity profile for a DMPC sample which was produced by Songbo Zheng.

All other data was collected and analyzed by Amit Patel.

Introduction:

1) Biological Background

1. 1) Biological Importance of Cell Death

In the lives of multicellular organisms, life and death is not only decided by the macroscopic world, but also the microscopic, at the level of the individual cells and molecules that the organism is comprised of. Counter intuitively, at this scale, the regulation of cell death (both for and against) is essential for the growth, development, and survival of the organism as a whole. During the embryonic stages of life, a fine balance between cell division and cell death defines the development of tissues and organs [Danial, 2004, Twomey, 2005]. This is also true for the maintenance of regular homeostasis within an organism, insuring that no subgroup of cells over or under proliferates. In addition, cell death is also used as a survival response towards mutations, defects, or infections that have permeated into the cellular structure of an organism. The importance of this role is felt strongly within the human population, as a deficiency in cell death may result in autoimmunity, while excessive cell death may result in degenerative diseases and infertility. In addition, the uncontrolled proliferation of malfunctioning or mutated cells via a deficiency in cell death can result in what Statistics Canada has shown to be the leading cause of human deaths in Canada, cancer. Even more alarming, between the years of 2000 and 2009, the number of deaths due to cancer steadily increased along with the mortality rate of patients with the disease. This alone emphasizes the importance

of increasing our understanding of cell death and the mechanisms responsible for its regulations.

1.2) Variety in Cellular Death Pathways

There are two basic categories of cell death, necrosis (Figure 1) and physiologically driven cell death. Necrosis is largely involuntary and often the result of cellular injury, resulting in degradation of its contents, swelling and eventual rupture, releasing its contents into the extracellular matrix [Danial, 2004]. The latter is further subdivided into three types, defined by their physical manifestations; heterophagic, autophagic, and non-lysosomal [Twomey, 2005]. Heterophagic responses are more commonly known as apoptosis (Figure 1) and require only the cell being acted upon [Danial, 2004]. Apoptosis is characterized by condensation of the chromatin, shrinkage and compartmentalization of the cell, followed by phagocytosis of the smaller vesicles by neighbouring cells for disposal or reuse of the contents [Twomey, 2005; Danial, 2004]. As apoptosis is a self-mediated form of cell death and is linked to cancer, it is often a topic of great interest in the research community.

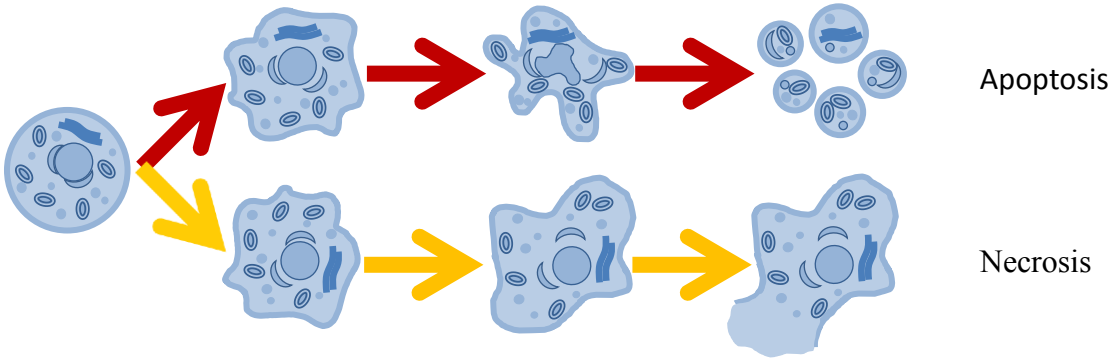

Figure 1: Structural Differences Between Apoptosis & Necrosis. Apoptosis is a form of cell-regulated death which results in the compartmentalization and dispersion of a cell and its contents. These smaller apoptotic bodies are either digested or incorporated into surrounding cells. In contrast to apoptosis, necrosis is generally results from injury to a cell, causing the cell to swell and burst, releasing its contents into the extracellular matrix.

1.3) Apoptotic Pathways

Considering the importance of apoptosis, it is present in a wide variety of species, and more interestingly, is largely conserved between them [Twomey, 2005; Danial, 2004]. In addition, species with greater complexity are observed to have a higher count of protein variety involved in the regulation of apoptosis. Therefore, it is essential to focus in on key stages of apoptosis allowing for the greatest impact on multiple pathways leading to cell death. One such stage at which many pathways converge involves the mitochondria and the Bcl-2 family of proteins. The Bcl-2 family members have been shown to regulate mitochondrial homeostasis and the containment and release of proapoptotic factors contained within the intermembrane space (IMS) as well as the mitochondrial inner membrane (MIM) (Figure 2). Once proapoptotic factors are released into the cytosol of the cell, it is committed to cellular death.

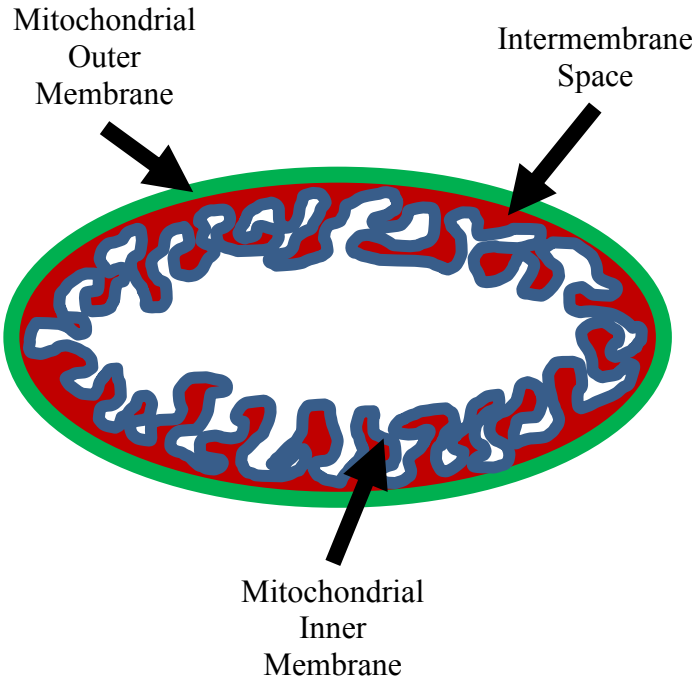

Figure 2: Artistic Rendition of Mitochondria. Mitochondria are unique organelle, housing their own DNA, separate from the rest of the cell. Mitochondria are also responsible for production of the majority of adenosine triphosphate found in the cell via cellular respiration. There are two sets of cellular membranes, the inner membrane and the outer membrane. The inner membrane forms structures known as cristae in order to increase surface area. Between the two membranes, there are molecules, such as cytochrome c, which are important for cellular respiration as well as apoptosis.

1.3.1) Bcl-2 Family Proteins Pathway Overview

Over the years, there has been much research put forward into understanding the mechanisms involving the Bcl-2 family of proteins and apoptosis. In general, there are three basic stages related to apoptosis; initiation, commitment, and execution. Initiation may occur in numerous ways via processes such as extracellular signalling. The Bcl-2

family of proteins however are involved in the commitment stage, the point after which, the cell can no longer abort cell death [Leber, 2007; Leber, 2010]. After the initial onset of apoptosis, caspases are activated via cleavage and eventually activate the sensitizer proteins of the Bcl-2 family of proteins such as Bid [Danial, 2004; Martinou, 2011; Petros, 2004]. Following cleavage, cleaved-Bid (cBid) translocates to the mitochondrial outer membrane (MOM). The two fragments then separate and the larger fragment, now denoted truncated-Bid (tBid), inserts into the MOM. After insertion, Bid recruits proapoptotic proteins, such as Bax, to the MOM, which proceed to insert and oligomerize into pores, thus causing MOM permeabilization (MOMP). Following MOMP, proapoptotic factors (such as cytochrome c) are released from the IMS into the cytosol, sealing the cell's fate. Several models have been put forward, such as the Direct Activation Model and the Displacement Model to explain the details of this step of apoptosis, though they have failed to explain all of the newly acquired observations. More recently, Leber, Lin and Andrews proposed the 'Embedded Together Model' (ETM). The ETM made key alterations to previous models to account for recent advances in apoptosis research, recognizing that several steps within the signalling pathways of apoptosis are in equilibrium, constantly activating and inhibiting one and another [Leber, 2007; Leber, 2010]. The cell is not committed to death until the Bcl-2 family proteins Bax and or Bak insert several helices into the MOM and oligomerize to form pores, causing MOMP. The ETM also acknowledges the similarity in structure and mechanism between Bcl-2 family proteins with similar functions. Finally, and perhaps most importantly, the ETM model acknowledges the importance of the lipid matrix of the

membrane and its effects on the resultant conformational changes in the Bcl-2 family of proteins to either advance or halt apoptosis. For this reason, studies of the membrane matrix are incredibly important to the understanding of the Bcl-2 family of proteins mechanisms.

1.3.2) Bcl-2 Family Protein Structures

The Bcl-2 family of proteins have been studied with great depth, and many studies have looked at their structures, functions and interactions. The family name follows from the first of the proteins to be discovered, the Bcl-2 protein, which was observed to block apoptosis from several different stimuli [Danial, 2004]. Other members were added as it was discovered that they presented homology to this initial protein. The sequence similarities that arise within this family have come to be known as the Bcl-2 Homology (BH) regions, of which there are 4 (Figure 3) [Twomey, 2005; Danial, 2004; Martinou, 2011; Petros, 2004]. The Bcl-2 family of proteins is broken down into 2 main subcategories; proapoptotic and antiapoptotic proteins (Figure 3 and Table 1). As their names suggest, the former refers to proteins that generally proceed to the activation of apoptosis, while the latter tends to help avoid cell death. Antiapoptotic proteins have all four of the BH domains (BH1 – 4) present [Martinou, 2011; Chipuk, 2008; Harris, 2000]. Proapoptotic proteins are further subdivided into two categories; the first containing BH1 – 3 regions and the other containing only the BH-3 region [Danial, 2004; Martinou, 2011; Chipuk, 2008; Harris, 2000]. The BH3-only proteins carry death signals from other cellular events either directly to the other BH1-3 pro-apoptotic proteins (in which case

they are called activators) or by inhibiting anti-apoptotic proteins (in which case they are called sensitizers). All of these proteins communicate with other proteins through their BH1, BH2 and most importantly, BH3 domains [Twomey, 2005; Danial, 2004].

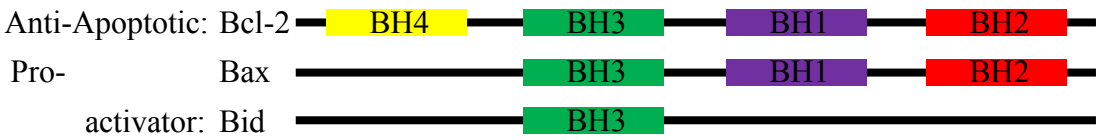

Figure 3: Bcl-2 Homology (BH) Regions. Simplified figure showing general trends between different Bcl-2 proteins. Anti-apoptotic proteins, such as Bcl-2, contain all four BH regimes; pro-apoptotic contain BH1-3, such as Bax, while sensitizers, such as Bid, poses only the BH3 domain.

Pro-apoptotic	Sensitizers	Anti-apoptotic
Bax	Bid	Bcl-xl
Bak	Bim	Bcl-2
	Puma	Mcl-1
	Bik	
	Noxa	
	Bad	

Table 1: Examples of Bcl-2 Proteins. Bcl-2 proteins are classified into three major subgroups dependent on their function; pro-apoptotic, sensitizers, and anti-apoptotic. Pro-apoptotic proteins, such as Bax induce apoptosis, but require an activator, such as Bid. Anti-apoptotic proteins inhibit apoptosis via interactions with sensitizers or pro-apoptotic proteins. Sensitizers mediate both pro- (green) and anti- (red) apoptotic proteins in order to control the onset or suppression of cell death. Dependent on the state of the cell, this may require the activation of pro-apoptotic proteins and/or the inhibition of anti-apoptotic proteins.

1.3.3) Bid: Structure and Function

With respect to the activation of apoptosis, the proapoptotic protein Bax and its activator Bid are two of the most important in the Bcl-2 family. As such, much of the research conducted within our lab is focused around these two members. Bid's sequence, as other BH3-only member, contains only the BH3 domain, which is essential for its function [Danial, 2004]. Bid consists of two central hydrophobic α-helices (αH) encompassed by six amphipathic αHs [Petros, 2004]. In a healthy cell, Bid remains within the cytosol in its inactive form. Prior to cleavage, αH1 of Bid has hydrophobic interactions with the BH3 region of the protein, resulting in its inability to interact with other Bcl-2 family proteins. Upon reception of a death signal, caspase 8 cleaves Bid upstream of the BH3 sequence into 2 fragments, which remain localized together until they are within proximity of the MOM [Petros, 2004; Liu, 2005]. Once in range, the two fragments separate, and tBid is inserted into the MOM ready to recruit Bax [Martinou, 2011]. Bid and Bax's interactions are believed to occur through their BH3.

1.3.4) Bax: Structure and Function

Bax is a proapoptotic Bcl-2 protein with BH1-3 regions [Petros, 2004]. In solution, Bax consists of two central hydrophobic αHs surrounded by seven amphipathic αHs. αH1 and αH2 are connected via a long unsaturated loop. αH2-4 compose a hydrophobic grove within the protein, and hydrophobic αH9 binds into the grove to shield them all to increase solubility in the cytosol [Petros, 2004; Danial 2004]. Despite this, Bax has been

observed to continuously translocate from the cytosol to the MOM and vice versa; only-showing preference for the MOM during apoptosis [Martinou, 2011; Danial 2004]. Some triggers involved in these translocations may be: other Bcl2-proteins, prostaglandins, p54, or pH variations or the structure of the MOM itself. Once Bax has been recruited by tBid to the MOM, the conformational changes induced via this interaction cause αH5 and αH6 to insert into the MOM and self-oligomerize with other Bax proteins to form a pore and cause MOMP [Leber, 2007; Martinou, 2011]. The types of pores formed by Bax has been under debate for some time, with some earlier evidence pointing towards a proteinaceous pore, but more recent research leaning towards a lipidic pore [Basañez, 2002; Martinou, 2011].

1.4) Lipids and Pore Formation

All lipids are amphiphilic molecules, composed of a hydrophilic head and hydrophobic hydrocarbon tails. This structure causes lipids to naturally form structures such as micelles, vesicles, and bilayers in an aqueous environment. In a purely lipid bilayer, pore formation and stability is determined by the balance of two main factors; the membrane tension and the line tension [Huang, 2004]. The membrane tension increases pore size, while the line tension decreases it. Pore forming proteins either induce the formation of a proteinaceous or lipidic pore (Figure 4). Porteinaceous pores are completely composed of proteins which span the thickness of the lipid bilayer, requiring little or no bending of the bilayer itself. In contrast, proteins involved in lipidic pores may not be completely transmembrane, and require the pores to be partly composed of lipids, requiring bending

of the bilayer. Therefore, it is reasonable to assume that the role of proteins that form lipidic pores is to favour membrane tension or decrease line tension during formation, and then induce an equilibrium between these two components to stabilize the pore. In lipidic pore forming antimicrobial peptides, several properties have been observed, and are likely present in the pore formation of Bax. Protein orientation in the membrane seems to be dependent on the concentration of proteins on the bilayer, with lower concentrations resulting in protein helices orienting parallel to the lipid bilayer. Once concentrations have reached a critical value, proteins begin to insert into the membrane, now parallel to lipid molecules and induce pore formation. It was also observed that positive lipid curvature assists pore formation as it reduces bending energy for the outer leaflet of the bilayer. Lipidic pore formation has also been observed to cause bilayer thinning [Huang, 2006; Lee 2008]. Recent research has shown that the lipid composition of the MOM in which the Bcl-2 proteins interact is also important to their function [Luken-Ardjomande, 2008; Basañez, 2002; Heit, 2011, Liu, 2006].

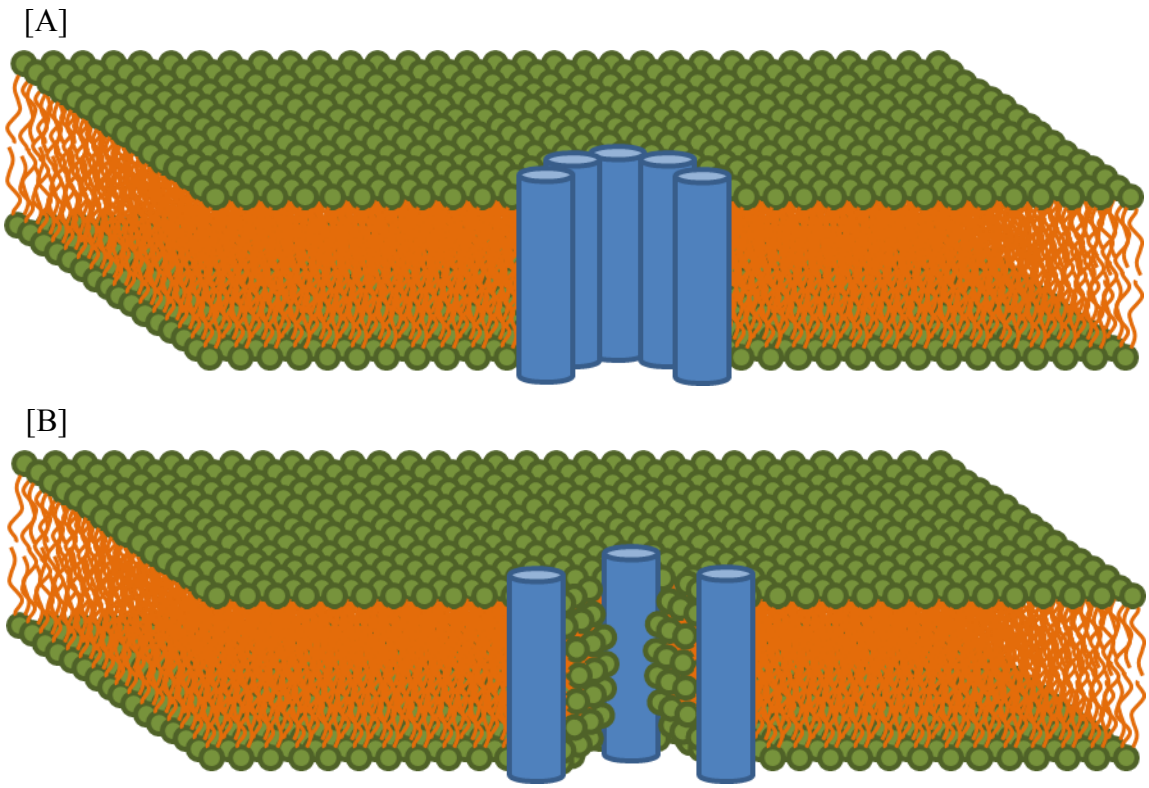

Figure 4: Artistic Rendition of Pore Types. Green circles are representative of lipid head groups, while orange tails are representative of lipid tails (hydrocarbon chains). Pore forming proteins are represented by blue cylinders. [A] Barrel-stave model representation of a proteinaceous pore. [B] Toroidal model representation of a lipid pore. Note the curvature of the lipid bilayer system, negative curvature about the circumference of the pore and positive curvature perpendicular to the membrane.

1.5) Mitochondial Outer Membrane

Due to the complexity of the MOM in vivo, it is important to isolate the important components and prepare a model system to study the system in a controlled environment. In the case of the Bcl-2 family of proteins, the importance of the lipid matrix of the MOM has been well established due to their formation of lipidic pores. Lipidic pores depend more heavily on the lipid composition as the membrane needs to bend to form these kinds

of pores and the bending energy of the membrane is directly linked to the intrinsic curvature of the lipids it is composed of [Basanez, 2002]. The five lipids present in the MOM model system used are based on *Xenopus* mitochondrial membrane and have been proven to effectively allow pore formation by tBid and Bax [Kuwana, 2002; Yethon, 2003]. This model membrane consists of Phosphatidylcholine (PC), Phosphatidylethanolamine (PE), Phosphatidylinositol (PI), Phosphatidylserine (PS), and Cardiolipin (CL) in the molar ratios of 48:28:10:10:4. The chemical structures of all five lipids and cholesterol are shown in Table 2. Of the five lipids, PE possesses a negative intrinsic curvature, PI is the only single chain polyunsaturated lipid, PS has a negatively charged headgroup and CL possess both a negative curvature and charge. PC is the least interesting as it has no distinguishing properties that have been attributed to the function of the Bcl-2 family of proteins. PE's negative curvature, as for antimicrobial peptides, has been shown to inhibit Bax oligomerization, but has no effect on the insertion of Bax into the MOM [Basanez, 2002; Luken-Ardjomande, 2008]. In order for PE to successfully inhibit Bax oligomerization it requires a concentration of at least 20%. Although PE doesn't seem to affect the binding of Bid after cleavage, it is unable to induce a separation of the two fragments as is necessary for its function [Liu, 2005]. In addition to curvature, lipid charge also plays a key role in membrane protein interaction. Apoptotic mitochondria dramatically increase their surface charge through lipids such as PS and CL [Heit, 2011]. Early on, the PS content of the cytosolic leaflet of the MOM increases, while PI content drops; though the charge increase has been linked more to the presence of increasing amounts of CL. Interestingly, CL tends to cluster and may offer a

stage for active caspase 8, which subsequently activates Bid. Upon activation, tBid has been shown to target CL in the MOM. tBid has also been observed to be able to induce these changes in the surface charge of the MOM. Bid and Bax activity has also seen to be concentrated near mitochondrial fission site, though their curvature seems to have little to do with this [Lucken-Ardjomande, 2008]. This phenomenon has been linked more closely to the possible transition of CL from the MIM to the MOM at sites of direct contact [Lucken-Ardjomande, 2008; Sorice, 2009]. Despite some of the conflicting data presented, charge and curvature of the lipid bilayer have a clear effect on apoptosis via Bid and Bax.

Molecule	Structure
PC (egg, chicken)	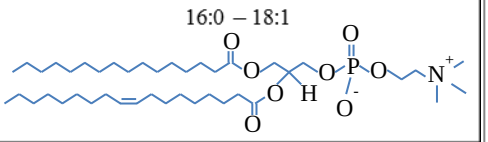
PE (egg, chicken)	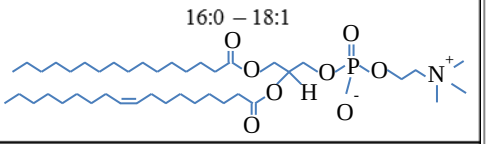
PI (liver, bovine)	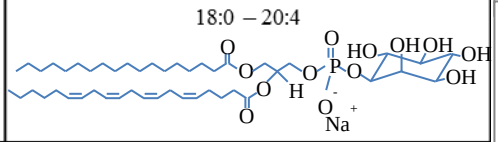
DOPS	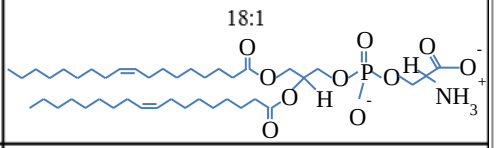
TOCL	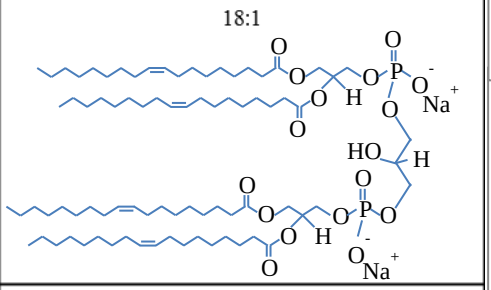
Cholesterol	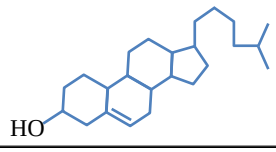

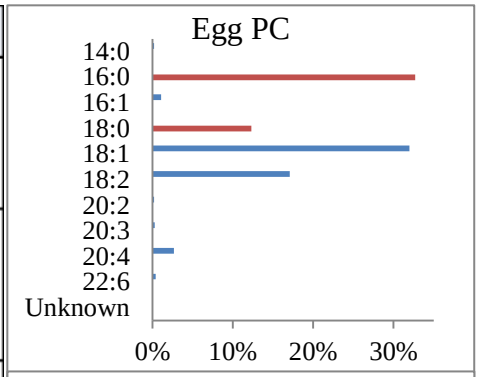

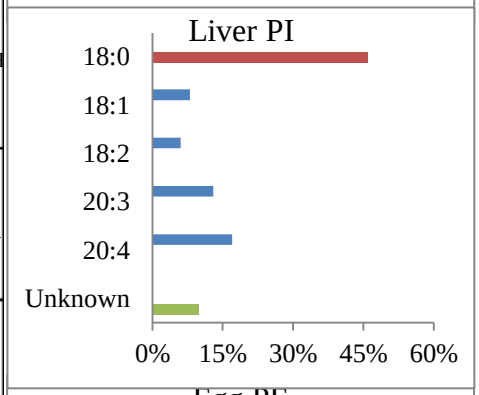

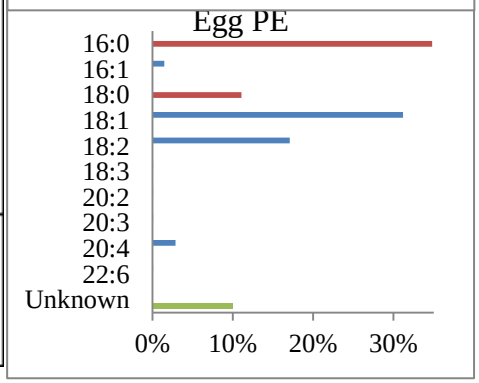

Table 2: Lipid and Cholesterol Structures and Distributions. PC, PE and PI purchased from Avanti Polar Lipids were extracted from natural sources; provided in brackets. Structures in the second column were acquired from the avantilipids.com and represent the dominant strain within the sample. Distribution of variants (also acquired from avantilipids.com) found within a sample are shown in the third column. The y-axis represents the tail length, given as (number of carbons):(number of double bonds). Red bars represent saturated hydrocarbon chains, blue bars represent unsaturated hydrocarbon chains, and green for unknown. The length of the bar, and the number at the end, represent the percentage presence for a given hydrocarbon chain within the sample. Average molecular weights for the phospholipid solutions are also given in the bottom right of each graph. These plots represent the presence of specific tails within a sample, though they do not show the combination required per molecule.

1.6) Cholesterol and Membranes

Cholesterol is another component of membranes than can have dramatic effects on its structure and properties and is predominately (80% to 90% of total cellular content) found in the cellular plasma membrane [Lange, 1983; Colbeau, 1971]. The plasma membrane has a cholesterol concentration of about 45%, whereas organelles such as the endoplasmic reticulum has between 10% to 12% [Yeagle, 1985; Colbeau, 1971]. The MIM and MOM were found to have 3% to 4% and 6% to 25% respectively, dependent on the species examined [Colbeau, 1971]. Cholesterol also has an amphiphilic structure (Table 2) which associates well with lipids. In contrast to Bax, which induces bilayer thinning, cholesterol tends to thicken the bilayer globally with increasing concentration [Hung, 2007; Satsoura, 2011]. The thickening process is nonlinear with respect to the cholesterol concentration and is only present until a threshold concentration is reached. Accompanying bilayer thickening, the density of lipids in the plane of the bilayer is increased and is known as 'the condensing effect' of cholesterol. Due to cholesterols amphiphilic structure, they naturally align parallel to the lipids of the bilayer with the hydrophilic and hydrophobic regions matching that of the lipids [Ivankin, 2010]. At low concentrations, cholesterol sits deeper inside of the bilayer as the hydrophilic headgroups of their neighbouring lipids shield cholesterol's hydrophobic regions from the aqueous environment. After a threshold concentration is reached, cholesterol shifts away from the hydrophobic core, and it's hydrophobic region is now shielded by the hydrophobic tails of surrounding lipids. At these high concentrations, above the membranes saturation limit (~40%),

cholesterol begins to form exclusive domains [Hung, 2007; Ivankin, 2010]. It is important to note, that the position of the cholesterol perpendicular to the plane of the membrane may shift globally or only for cholesterol outside of the cholesterol rich domains depending on the bilayer composition. In addition, the presence of multiunsaturated lipids has been shown to cause cholesterol to align parallel to the plane of the lipid bilayer and sit deep inside the hydrophobic core [Kučerka, 2009]. Cholesterol is also known to increase membrane rigidity, presumably by positioning within the bilayer and restricting lipid tail fluctuations [Hung, 2007].

1.7) Bcl-2 Family Proteins, Lipids, and Cholesterol Interactions

In the case of the Bcl-2 family of proteins, it is clear there is much debate within the scientific community on the roles of the MOM and its lipid constituents on the functioning of Bid and Bax. In addition to lipids, cholesterol has also been noted to be a strong determinant of whether Bax will be able to form pores within the MOM. Increased concentrations of cholesterol have been noted to inhibit tBid-induced pore formation by Bax [Luken-Ardjomande, 2008*]. Counter intuitively, cholesterol may increase Bax insertion into the MOM, but reduces Bax oligomerization, and thus inhibit pore formation. Meanwhile, other studies have shown that cholesterol may in fact improve Bax and its translocation to the MOM, but inhibit its insertion into the lipid bilayer [Christenson, 2008; Martinez-Abundis, 2009]. In order to further investigate this system, and perhaps help to clear up some of the controversy surrounding the connections between lipids, cholesterol and the Bcl-2 family of proteins, several studies conducted in

our group by Shamas-Din et al. (yet to be published) have examined the effects of varying the composition of lipids in the MOM-like lipid mixture. A portion of this work further explored the relationship between cholesterol and Bax (Figure 5), once again, showing an inhibitory effect on membrane permeabilization by tBid and Bax. In order to determine which step of pore formation was affected, several further studies were conducted. They showed binding of cBid to the membrane was unaffected by cholesterol concentration. Cholesterol content was responsible for slower rates of interaction between tBid and Bax, though the extent of interaction remained unchanged given sufficient time and is thus unlikely to be responsible for inhibition of pore formation. Ruling out the two aforementioned steps, Bax insertion was shown to decrease with increased cholesterol concentration. Regardless of the exact reasoning, a link between cholesterol content and pore formation is certain, though it is yet unclear whether this effect is due to chemical interactions or due to structural changes to the bilayer or both. This thesis strives to explore structural changes to the MOM and attempts to link its connection with Bax pore formation.

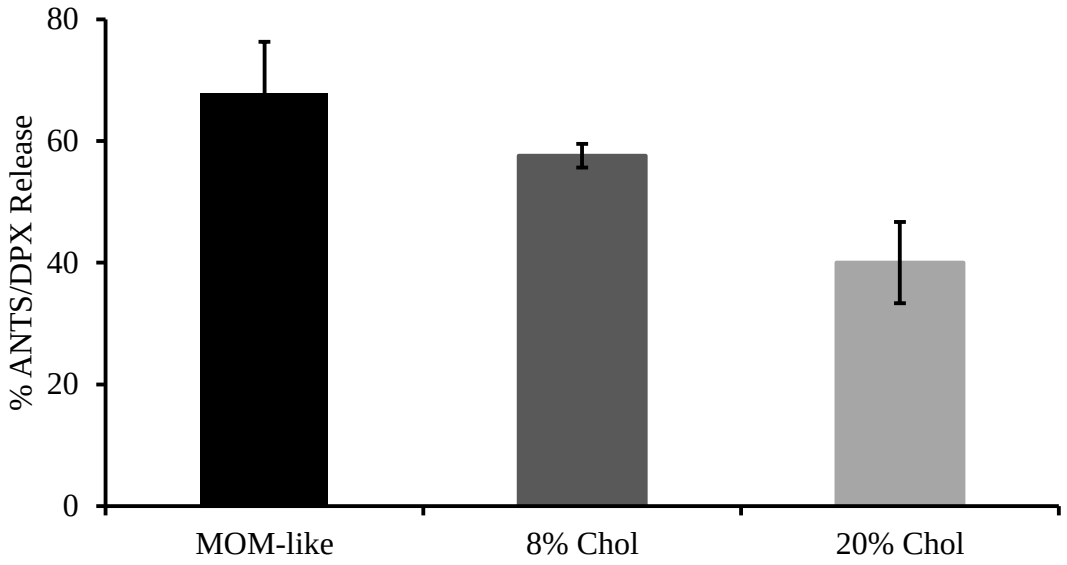

Figure 5: Cholesterol Effects on Bax Pore Formation. Data collected by Aisha Shamas-Din. Liposomes with indicated lipid compositions were encapsulated with ANTS and its quencher DPX, and incubated with 100nM Bax and 20nM tBid. Due to the close proximity between ANTS and DPX within the liposome, low levels of fluorescence is observed, however, upon release into the solvent via Bax pores, ANTS is no longer in proximity of DPX and thus results in an increased fluorescence signal. Lower fluorescence signals therefore signify a decrease in Bax pore formation.

1.8)Model System: Solid Supported Lipid Bilayers

A cellular membrane has a highly complex mix of components, including lipids, cholesterol, and various proteins to name a few. The complexity of the system makes it very difficult to understand the interactions between components directly; because of this, it becomes essential to simplify the naturally occurring system to a model system composed of only components of interest. In the case of the Bcl-2 family of proteins, it is clear that there is a connection between the lipid composition of the MOM and the functioning of Bid and Bax.

Solid supported lipid bilayers (SSLB) prove to be an ideal model system in order to study the structure of lipid bilayers and their constituents. In contrast to liposomal bilayers in solution, this system consists of one or more planar bilayers stacked on top of a solid support, such as silicon wafers, quartz, mica, or glass to name a few. There are many benefits in utilizing SSLB systems. The macroscopic size of the system allows for easy production and physical manipulation in the lab, including storage and orientation during experiments. These systems have also proven to be very stable and are able to be kept for lengthy period of times, ranging from a few days to months depending on the lipid composition and storage environment. These systems are also well oriented and are thus ideal for structural probing through techniques such as atomic force microscopy and x-ray (or neutron) scattering. It is also important to note that Bax has been shown to be able to form pores within these system, giving a biological significance to their study [Martinou, 2011]. SSLBs can be prepared with either a single layer through processes such as vesicle fusion, or multiple layers ranging from a few, using techniques such as Langmuir-Blodgett deposition or spin coating, to thousands using techniques such as lipid deposition, in which lipids dissolved in solution are allowed to deposit individually onto a substrate/lipid layer until all lipids have deposited.

Materials & Methods:

2) Materials

2.1) Solid Support: Silicon

Silicon wafers were purchased from Silchem Handelsgesellschaft mbH (www.silchem.de) based in Germany. Wafers had a (1 1 1) orientation and were polished on one side. The resistivities measured less than 0.016 Ohmcm. The 300 μm thick wafers were laser cut to 1 cm by 1 cm squares by the supplier.

2.2) Chemicals & Salts

Several chemical products were used throughout sample preparation and data collection procedures. During sample preparation; 98% hydrogen peroxide (H_2O_2), 30% sulphuric acid (H_2SO_4), 98% (3-Aminopropyl)triethoxysilane (APTES), and chloroform were used, while several different salts were used as hydration buffers during data collection. H_2O_2 is a weak acid with oxidizing properties and is often used as a cleaning agent due to its detergent like behaviour. H_2SO_4 is a strong corrosive acid capable of oxidization and is thus very useful in the cleaning of substrates. APTES binds well to the surface of silicon wafers and provides a hydrophobic surface via its short hydrocarbon tail. Chloroform is an organic compound that is often used to mix and store a variety of lipids as they are all able to efficiently dissolve into this solvent. Salts can be used to effectively moderate the humidity within a controlled environment by supersaturating the water supply. The four salts used in this work were sodium chloride (NaCl), potassium chloride (KCl), potassium

nitrate (KNO_3), and potassium sulphate (K_2SO_4). The relative humidity produced by these salts can be found on the omega website (omega.com) with their results summarized for experimental conditions used in this thesis in Table 3.

Temperature (°C)	Sodium Chloride	Potassium Chloride	Potassium Nitrate	Potassium Sulphate
10	75.67 ± 0.22	86.77 ± 0.39	95.96 ± 1.4	98.18 ± 0.76
15	75.61 ± 0.18	85.92 ± 0.33	95.41 ± 0.96	97.89 ± 0.63
20	75.47 ± 0.14	85.11 ± 0.29	94.62 ± 0.66	97.59 ± 0.53
25	75.29 ± 0.12	84.34 ± 0.26	93.58 ± 0.55	97.30 ± 0.45
30	75.09 ± 0.11	83.62 ± 0.25	92.31 ± 0.60	97.00 ± 0.40
35	74.87 ± 0.12	82.95 ± 0.25	90.79 ± 0.83	96.71 ± 0.38
40	74.68 ± 0.13	82.32 ± 0.25	89.03 ± 1.2	96.41 ± 0.38

Table 3: Relative Humidity Induced by Salts. Supersaturating water reservoir with a salt may reduce the relative humidity of the environment. This effect is also temperature dependent and is shown for a range of temperatures and salts relative for this work. The relative humidity is provided as a percentage with respect to the humidity of an environment without a salt in the reservoir.

2.3) Lipids and Cholesterol

All lipid and cholesterol products were purchased from Avanti Polar Lipids, inc. (avantilipids.com). The chemical names (and catalogue numbers) of purchased PC, PE, PI, PS, and CL purchased are L-α-phosphatidylcholine (840051), L-α-phosphatidylethanolamine (841118), L-α-phosphatidylinositol (840042), 1,2-dioleoyl-sn-

glycero-3-phospho-L-serine (840035), and 1',3'-bis[1,2-dioleoyl-sn-glycero-3-phospho]-sn-glycerol (710335) respectively. All lipids were purchased in a chloroform solution. The majority of lipids purchased (PC, PE, and PI) are extracted from natural sources, which means that a mix of lipids are in fact present in the samples. Table 2 shows both the structure of the dominant species present in these natural lipids as well as the distribution of the lipids present. The properties discussed below refer to the dominant species within the samples. PC was extracted from chicken eggs and the main species has 16:0-18:1 hydrocarbon chains with the double bond on the ninth carbon (Tables 2 and 4). The PE purchased was transphosphatidylated from egg and also has mainly 16:0-18:1 hydrocarbon chains with the double bond on the ninth carbon (Tables 2 and 4). PI is the only single chain polyunsaturated lipid used and was extracted from bovine liver with 18:0-20:4 hydrocarbon chains with double bonds on the fifth, eight, 11^{th}, and 14^{th} carbons. PS used was produced synthetically with 18:1 hydrocarbon chins, both double bonds on the ninth carbon. CL is the only lipid with four hydrocarbon chains, all of which are 18:1 carbons long with the double bonds on the ninth carbon of each chain. Cholesterol (700000P) from ovine wool was also purchased from Avanti Polar Lipids. In contrast to the five phospholipids used, cholesterol consists of four linked hydrocarbon rings, with a hydroxyl group (polar) at one end and a short hydrocarbon tail at the other. Cholesterol was purchased as a powder dissolved in chloroform prior to mixing with the other lipids. It is important to note that aliquots (roughly 200μL) of the individual lipids were prepared to prevent contamination of the stock solutions as well as major concentration changes due to chloroform evaporation. The cholesterol was first dissolved

in chloroform to a concentration of 10 mg/mL, and was later aliquoted prior to use. During aliquoting, a glass and metal syringe was used to prevent contamination of lipid solutions from reactions between the chloroform and plastic pipette tips. In addition, a low argon flow was utilized to prevent any exposure of solutions to oxygen in the air, which would otherwise degrade the unsaturated lipids. The rate of argon flow was kept low so as to prevent excessive evaporation of chloroform. Stock solutions and aliquots were stored in a +4°C incubator with vials filled with argon gas to prevent lipid degradation.

Lipid	Tails	Curvature	Charge
PC	16:0 – 18:1 (9)		
PE	16:0 – 18:1 (9)	Negative	
PI	18:0 – 20:4 (5,8,11,14)		-1
DOPS	18:1 (9)		-1
TOCL	18:1 (9)	Negative	-2

Table 4: Lipid Properties. Tail lengths are representative of the dominant species within a sample, with numbers in brackets representing the position off the double bond in the hydrocarbon chain, with the first carbon being closest to the head group. Curvature and Charge of lipids is provided for each lipid as they are the most important properties of the lipids with respect to the Bax and Bid. PE and TOCL both possess negative curvature, with head groups occupying a larger area than the hydrocarbon tails perpendicular to length of the lipid. PI, DOPS, and TOCL have negatively charged phosphate head groups, with TOCL possessing a charge of -2.

3) Methods

3.1) Lipid & Cholesterol Solution Preparation

In order to prepare multilayer SSLBs, a protocol developed in Dr. Maikel Rheinstädter's group was adopted and modified for use with a MOM lipid mixture [Barrett, 2012]. Solution preparation was carried out by mixing the 5 lipids and cholesterol in chloroform with the desired molar ratios. In the case of the MOM-like samples, the ratios were 48:28:10:10:4 for PC:PE:PI:PS:CL respectively. Pure chloroform was later added to

achieve a final solution concentration of 15 mg/mL. All lipids were purchased dissolved in a chloroform solution with concentrations of 25 mg/mL for PC and PE and 10 mg/mL for PI, PS, and CL. The syringe was also washed a minimum of five times using pure chloroform to prevent any cross contamination of the lipid aliquots or stock solutions. With solutions involving cholesterol, the molar ratios of PE, PI, PS, and CL were conserved, and PC was reduced proportionally. In this way, the overall surface charge and intrinsic curvature of the membrane was conserved, since PC is a neutral lipid with negligible intrinsic curvature.

3.2) Silicon Substrate Preparation

The first step when preparing the silicon substrates for solution deposition, was to clean the silica substrates. The silicon wafers were placed into a solution (polished side up) of hydrogen peroxide and sulphuric acid in a ratio of 1:3. In preparing this solution, H_20_2 should always be added to the glass container first in order to prevent an aggressive reaction. This procedure is usually completed for 30 minutes at room temperature for lipids such as 1,2-dimyristoyl-sn-glycero-3-phosphocholine (DMPC). This procedure ensured the removal of organic contaminants from the substrates surface while also rendering it hydrophilic. Upon completion, wafers were removed from the bath to be rinsed by 3 cycles of ultrapure water then ethanol, each 10 seconds at a time. It is essential to prevent any exposure to air during this process so as to avoid contamination of the surface. Due to the use of chloroform solutions, deposition onto these freshly cleaned substrates resulted in severe dewetting caused by the repulsion between the

hydrophobic chloroform and the now hydrophilic silicon. In order to circumvent this issue, APTES was deposited onto the substrate. This is accomplished by preparing a 1% solution of APTES in ethanol and allowing the freshly rinsed wafers to bathe in the solution over night at room temperature. During this time period, the solution is continuously rotated on a platform to avoid settling of APTES, keeping the solution homogenous. Since ethanol is used as the solvent, during the rinsing prior to this step, it is essential that the last rinse be completed using ethanol so as to avoid the addition of water into the solution. Upon completion, wafers are removed and rinsed with ultrapure water and then methanol. This rinsing process is done three times, with the final rinse always being completed using methanol. Again, it is key to avoid exposure to air so as to not degrade the APTES. Wafers are dried using argon gas and annealed in vacuum for three hours at approximately 115°C. This procedure allows the APTES to uniformly layer on the substrate. Figure 6 shows the x-ray reflectivity profile of a silicon wafer with APTES on it. The broad peak is representative of a low number of layers of APTES present on the silicon wafer. After wafers have cooled, they are ready for lipid deposition to form well-ordered multilayers.

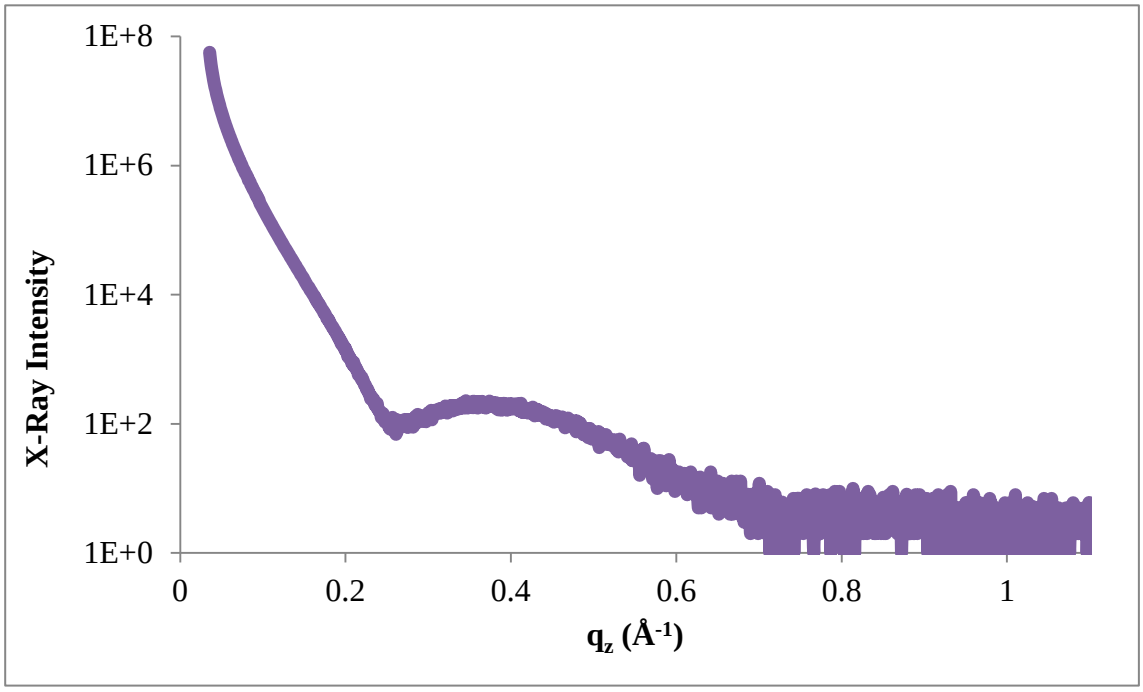

Figure 6: APTES Layer on Silicon Wafer. Silicon wafer was submerged in a 1% APTES solution overnight, and cleaned with methanol. X-ray reflectivity scan was completed immediately after cleaning at 22.5°C for 1 hour.

3.3) Sample Preparation: Lipid Deposition

In its most basic formation, lipid deposition requires the lipid-chloroform solutions to be deposited onto the prepared substrates and allowed to evaporate, leaving only lipid bilayers on the substrate. To begin, the solution to be deposited is extracted into a cleaned syringe (about 50 μL of the 15 mg/ml lipid solution for a 1 cm by 1 cm wafer), ready for deposition. Substrates are removed from vacuum storage and rinsed with pure methanol for roughly 20 seconds and subsequently dried under argon gas. Upon completion, the lipid solution is swiftly deposited onto the substrate to minimize exposure to air, and allowed to evaporate at 40°C. The enclosed environment chosen is a medium

sized petri dish, roughly 2 cm in diameter. Note that the samples are also elevated off of the base of the petri dish using a small metal washer to prevent the solution from flowing off of the substrate as well as to prevent the substrate from becoming fused to the petri dish. The use of a small enclosed environment allows for quick saturation of the enclosure with chloroform gas, slowing the evaporation of the solvent. This prevents internal currents and increasing concentrations of lipids from dictating the deposition of lipids, allowing them to form well oriented bilayers based on their interactions with the substrate or deposited layers. Samples are allowed to evaporate in this manner for roughly one hour before being vacuum annealed overnight at room temperature to extract all possible remnants of chloroform from the sample. Samples are then hydrated in 98% humidity through the use of potassium sulphate from 20°C to 30°C in increments of 1°C per hour. A slow rate of hydration is key to avoid bubbles from forming in the sample due to excessively fast hydration. This process allows lipids to enter a more fluid state and realign into perfectly oriented bilayers. Upon completion, samples may be removed and stored under argon gas in a +4°C incubator or removed for immediate experimentation. In the event that reflectivity profiles were less than satisfactory, the samples may be incubated at 50°C for 3 hours to improve bilayer orientation. Removal of samples from the hydration chamber results in almost immediate evaporation of the majority of the water in the sample, reducing it to the so called dry state.

3.4) Quartz Sample Protocol Adjustments

In addition to preparation of multilayer SSLB on silicon wafers, samples were also prepared on Quartz substrates. These substrates were roughly 2.5 cm in diameter and 2 mm thick. Preparation of the substrate was much simpler, requiring only rinsing with methanol, followed by a gentle scrubbing with a methanol soaked kim wipe. Samples were then dried under argon gas and lipid-chloroform solutions deposited using the exact same procedure as when preparing silicon wafers. Note that Quartz did not require any chemical alterations to prevent dewetting of chloroform.

3.5) X-ray Reflectivity

3.5.1) Instrument: B.L.A.D.E.

Taking advantage of the samples aligned planar geometry, x-ray reflectivity experiments were conducted to extract details of the structure of the membranes. Dr. Maikel Rheinstädter kindly allowed the use of his Rigaku SmartLab system, code named B.L.A.D.E. (Biological Large Angle Diffraction Experiments) and the sample chamber he designed (Figure 7). The sample chamber, depicted in Figure 7, is made of aluminum and kapton. Aluminum is largely opaque to x-rays but has a relatively low specific heat capacity allowing for accurate temperature control within the sample environment. Kapton is a synthetic material that is transparent for x-ray radiation, and is thus commonly used in chamber design. B.L.A.D.E. is a specialized instrument used for x-ray scattering experiments using a rotating CuK_{α} anode to produce x-rays with a wavelength of 1.5418 Angstroms (Å). B.L.A.D.E. sample alignment in the plane of the pedestal was

first done manually. The automated portion of the sample alignment then positions the sample into the center of the x-ray beam vertically (perpendicular to the plane of the pedestal) and aligns the surface of the sample surface to insure the plane of the sample surface is parallel to the beam. This process is repeated several times until the sample is fully aligned. In the study of SSLB systems, B.L.A.D.E. has an advantage over other instruments in the way it completes the reflectivity scans and orients the sample. The sample is placed horizontally rather than vertical, allowing for increased confidence in sample integrity, especially during hydration which may cause the sliding or washing away of layers in a vertical setup. In completing the reflectivity scans, the sample is held fixed in its aligned position while the x-ray source and detector are rotated simultaneously. This allows for incorporation of water into the chamber without fear of water running over the sample, as would be the case if the stage were to be rocked instead. To take full advantage of this system, a custom sample chamber consisting of aluminum and kapton was designed by Dr. Maikel Rheinstädter (Figure 7). This chamber provides an enclosed environment which allows for hydration of the sample through the addition of water and salts into a well surrounding the sample stage. In addition, a water channel below the base allowed for heating of the stage through conduction thus allowing controlled hydration and temperature within the chamber. In order to prevent condensation on the kapton windows due to temperature differences between the interior and exterior of the chamber, heated air was blown over the exterior of the windows according to the temperature inside the chamber as shown in Figure 7.

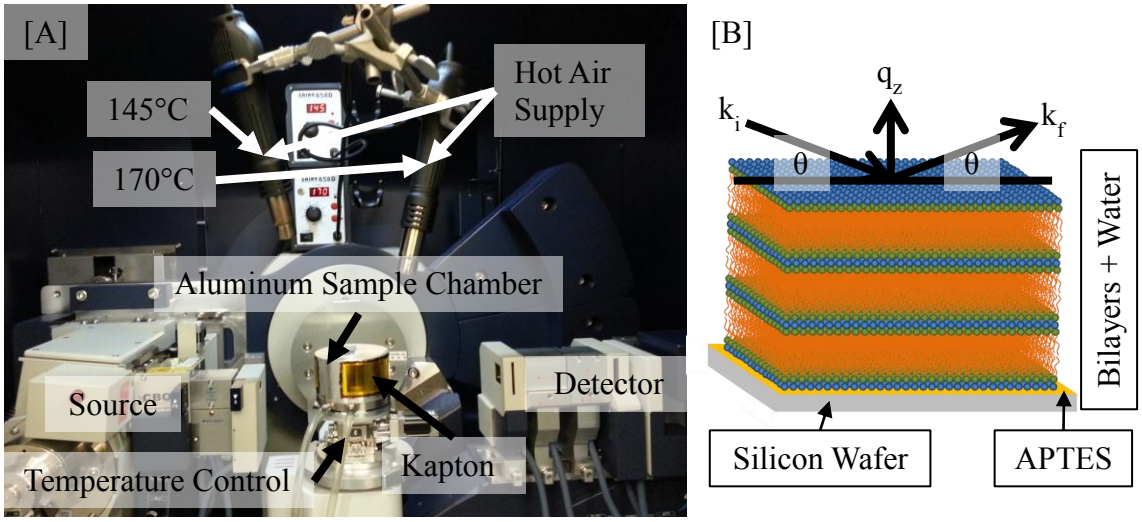

Figure 7: Experimental Setup and Geometry. [A] The Rigaku Smart Lab system, code named B.L.A.D.E. with sample chamber in place. During a specular reflectivity scan, the source and detector are moved in tandem, while the sample chamber is held stationary. The Sample chamber is composed of aluminum, with the addition of kapton windows to allow for the passage of x-rays to the sample within. The Humidity is controlled through the use of a well within the chamber where water is added with the desired salt for humidity control. In addition, the temperature is controlled by a enclosed water channel below the well as well as two hot air supplies above. The water channel control the temperature of the aluminum chamber, while the hot air supplies prevent condensation on the much thinner kapton windows. As one window is larger than the other (for in-plane scans), one hot air supply is set at 170°C on the larger window, and 145°C on the smaller window. [B] Geometry of a specular reflectivity scan on an artistic rendition of a SSLB, with the incident (k_i) and reflected (k_f) beams present, as well as the incident and reflected angles (θ). Since $|k_i|=|k_f|$, the momentum transfer vector is only in the perpendicular (z) axis and is labelled q_z. The grey slab is representative of the silicon wafer, with a layer of APTES (yellow) present on it, followed by multiple layers of MOM-like membranes and water between.

3.5.2) Reflectivity Measurements

Using the ability to move both the x-ray source and detector independently allowed scans to be conducted using a specular reflection geometry (2θ-scan). That is to say, both the incident beam and reflected beam being measured had the same angle with respect to the

plane of the sample. In doing so, we are able to scan over a small portion of the Ewald sphere. The Ewald sphere is a construct based on the concept of elastic interactions with both the incident and diffracted wave vectors having the same magnitude. As the diffracted radiation may go in any direction but always has the same magnitude, all possible positions for the end of the wave vector transfer creates a (Ewald) sphere.

There are two factors to be considered with respect to the experimental data collected using reflectivity: the Fresnel decay and the Lorentz correction factor [Daillant, 2009; Buerger, 1940]. For a perfect interface (an interface which is flat and has no mixing of the two substances) between two media, Fresnel's laws of reflection predict the amount of incident radiation that is reflected versus transmitted based on the refractive indices of the media and the angle of the incident radiation. Fresnel showed that there are 3 regimes of behaviour as a function of incident angles. The first regime shows perfect external reflection below a specific angle known as the critical angle (θ_c); the second shows a dependence based on Fresnel's reflectivity equation while the angle is lower than approximately three times θ_c; and in the final regime, Fresnel's reflectivity equation becomes approximately equal to $1/q_z^4$ (Figure 8). In addition to this intensity decay, the Lorentz correction factor is dependent on the specific geometry of the sample and manifests itself as a factor that needs to be added to the expression of the reflected intensity, and which is proportional to $1/\sin(2\theta)$ (or $1/q$ in reciprocal space) for oriented samples, as is the case for the work done in this thesis [Buerger, 1940; Kučerka, 2005].

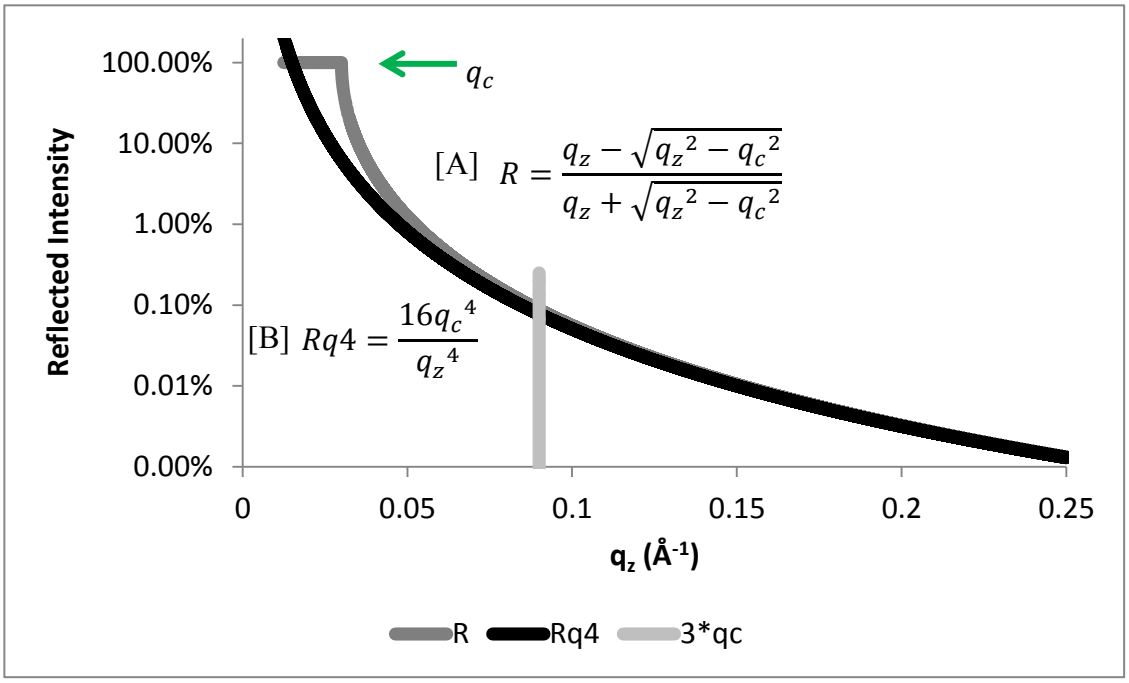

Figure 8: Fresnel Reflectivity Profile. Fresnel's equation for electromagnetic reflection off of an interface is given by equation [A] and plotted using a blue curve. A simplification of the equation is given by equation [B] and the red curve. As it can be seen, above approximately 3 times the critical angle (labelled q_c), the simplification becomes valid, and the reflectivity profiles simplifies into q_z^{-4}.

3.5.3) Data Analysis: Theory

The intensity data collected in a scattering experiment in reciprocal space (also known as momentum space) is representative of the electron density (ED) profile of the sample in real space (ρ). The two are related through the Fourier transform of the ED (Equation 1).

Equation 1: $$F(q_z) = \int_{-\infty}^{\infty} e^{iq_z z}\rho(z)dz$$

It is standard practice to convert angles (θ) into q_z (momentum transfer vector) notation to account for this fact. Equation 2 shows the relationship between q_z and θ, which is also dependent on the wavelength (λ) of radiation used during the experiment.

Equation 2: $$q_z(\theta) = \frac{4\pi sin\theta}{\lambda}$$

q_z is the vertical component of the momentum transfer vector shown in Figure 7 and is related to the unit cell length, d, in Bragg's Law by 2π/d. For a reflectivity experiment, the intensity of the reflected beam (R) is described by Equation 3, in which $S(q_z)$ is the structure factor, $F(q_z)$ is the form factor and $1/q_z$ is the standard Lorentz correction factor in reciprocal space notation.

Equation 3: $$R(q_z) = \frac{S(q_z)F(q_z)^2}{q_z}$$

The structure factor describes the scattering of a stack of interfaces, while the form factor is the Fourier transform of the ED profile of a single bilayer (Equation 1). As a consequence of the 2θ-scan geometry, structural information perpendicular to the plane of the bilayer (out-of plane) is collected. 2θ-scans using a single solid supported bilayer would provide the continuous form factor directly; use of a stacked geometry with repeating unit cells of size d_z collapses the form factor into discrete Bragg peaks. Bragg peaks result from constructive interference as described by Equation 4, where n is an integer.

Equation 4: $$2d_z \sin\theta = n\lambda$$

When the path difference, which changes with angle, is equal to an integer value of the wavelength of the incident beam, the diffracted beams will interfere constructively, resulting in what is known as a Bragg peak. This will occur at several different angles and is directly linked to the size of the repeating unit cell (the so-called d_z spacing). In a hydrated multilamellar sample, the unit cell consists of the bilayer as well as the water surrounding it. Using sampling theorem as described by King and Worthington, gathering reflectivity data of samples with different d_z spacing, while keeping the structure identical results in obtaining multiple sets of discrete points along the continuous transform $T(q_z)$ defined by Equation 5, where I_n is the integrated intensity of the n^{th} order peak at position q_n with phase v_n [King, 1971; Adachi, 2000]. The phase of the nth order peak is simplified to either +1 or -1 due to the centro-symmetry of a lipid bilayer in the q_z direction.

Equation 5: $$T(q_z) = \sum_n \sqrt{I_n q_n} v_n sinc(\pi d_z q_z - \pi n)$$

The points along the continuous transform can be obtained through hydration or dehydration experiments. Since whenever the continuous function $T(q_z)$ intercepts the horizontal (q_z) axis, the phase of the system changes; using this technique allows one to obtain the value of the phase depending on where a set of n^{th} order peaks resides.

Combining the above mentioned techniques, it is possible to extract the integrated intensities, corrected for background and geometric considerations, while also obtaining phase information, all of which is required to Fourier transform the form factor into the ED profile as per Equation 6. This discrete Fourier transform requires knowledge of the density of water (ρ_w), the 0^{th} order transform (F(0)), which is not directly observed in the reflectivity data collected, as well as all of the I_n and q_n values for all of the peaks (up to N) observed in the reflectivity data in order to calculate the ED on an absolute scale.

Equation 6: $$\rho(z) = \rho_w + \frac{F(0)}{d_z} + \frac{2}{d_z}\sum_1^N \sqrt{I_n q_n} v_n \cos\left(\frac{2\pi n z}{d_z}\right)$$

3.5.4) Data Analysis Software

In order to complete the data analysis process outlined above, a program was written using matlab and the Spec1D analysis suit developed by Des McMorrow and Henrik Rønnow at the Institute Laue-Langevin (ILL) in Gernoble, France. B.L.A.D.E.'s raw data output provided the intensity as a function of the angle between the source and detector (2θ), for which the angles were converted into the momentum transfer vector q_z through the use of Equation 2. The background was fit with a power law function proportional to $1/q_z^4$. Bragg peaks were first attempted to be fit using a Gaussian function, followed by a Lorentzian function, though both seemed inadequate at fitting all peaks properly. Gaussian fits tended to neglect the extended tails of peaks, while Lorentzian fits neglected widths of the peaks. In order to compensate for these shortcomings, a convolution of the two functions was used, the so called Voigt function.

In the event that this function was unable to properly fit any peak with a narrow base, the Gaussian function was used instead. In this way, all peaks of a single reflectivity profile were fit simultaneously with either a Voigt function or a Gaussian function over the background signal. In order to fit the raw data well, initial parameters needed for all peaks (amplitude, position, and width), as well as the background signal. Initial parameters for the background signal was constant regardless of reflectivity profile, though inputs for peaks needed to be inserted for each profile individually. In order to save time, peak positions and amplitudes were determined through the exploitation of their periodicity; a single peak was selected through graphical user input, which was then individually fit. Positions of all other peaks were extrapolated accordingly and data points closest to these values were used as the initial positions and amplitudes for the peaks. Initial peak widths were held constant for all peaks and profiles. Once all initial parameters were selected, the profile was fit using only the Voigt function to describe peak shapes with the Spec1D fitting routines. All peaks were then individually checked for accurate fitting and any poorly fit peaks were identified. The entire profile was refit using a Gaussian fit for peaks identified in the previous step, while all others were fit using the Voigt function. Upon completion, the area (I_n) and periodicity ($avg(q_z(n)/n)$) of Bragg peaks were calculated. The measured intensities were multiplied by q_z as well as an arbitrary scaling constant while the d_z spacing was evaluated by dividing 2π by the periodicity. This process was completed for several hydration levels using NaCl, KCl, and K_2SO_4 within run-through of the algorithm. Their values were then plotted for all possible combination and fit using the continuous function $T(q_z)$. The phase combination

that provided the best fit along with a small y-intercept value and a function which converged to 0 at large q_z, was selected for ED calculations. A discrete Fourier transform was conducted to extrapolate the ED profile (as per Equation 6) using Lorentz corrected intensities and the determined phases. Since F(0) was not determined experimentally, the ED profile was calculated on a relative scale, and so the profile was not shifted to the correct water density either.

Results & Discussion:

4) Sample Preparation Refinement

Utilization of the standard sample preparation protocol (Table 5) resulted in large variations in sample quality, from visually poor (opaque foggy white coloration) even after hydration of the sample, to ones with quality hydrated reflectivity profiles. Figure 9 displays an example of a spectrum of a MOM-like sample prepared using the standard protocol, which seemed visually acceptable (no opaque coloration) after hydration. In the dry state, the reflectivity profile shows severe peak splitting, representative of at least two different structures within the sample. In addition, when compared to the hydrated scan, one would expect the dry scan to have a larger number of peaks to be present at higher q_z due to the decreased kinetics (the hydrocarbon chains fluctuate slower) within the sample, which is not the case for the sample shown in Figure 9. This absence of higher order peaks in the dry state alludes to a disordered, inhomogeneous structure within the sample. Due to these deviations from what is considered a homogenous, well-ordered SSLB

system, the sample preparation protocol first needed to be refined before further experiments exploring the relationship between cholesterol content and membrane structure could be conducted.

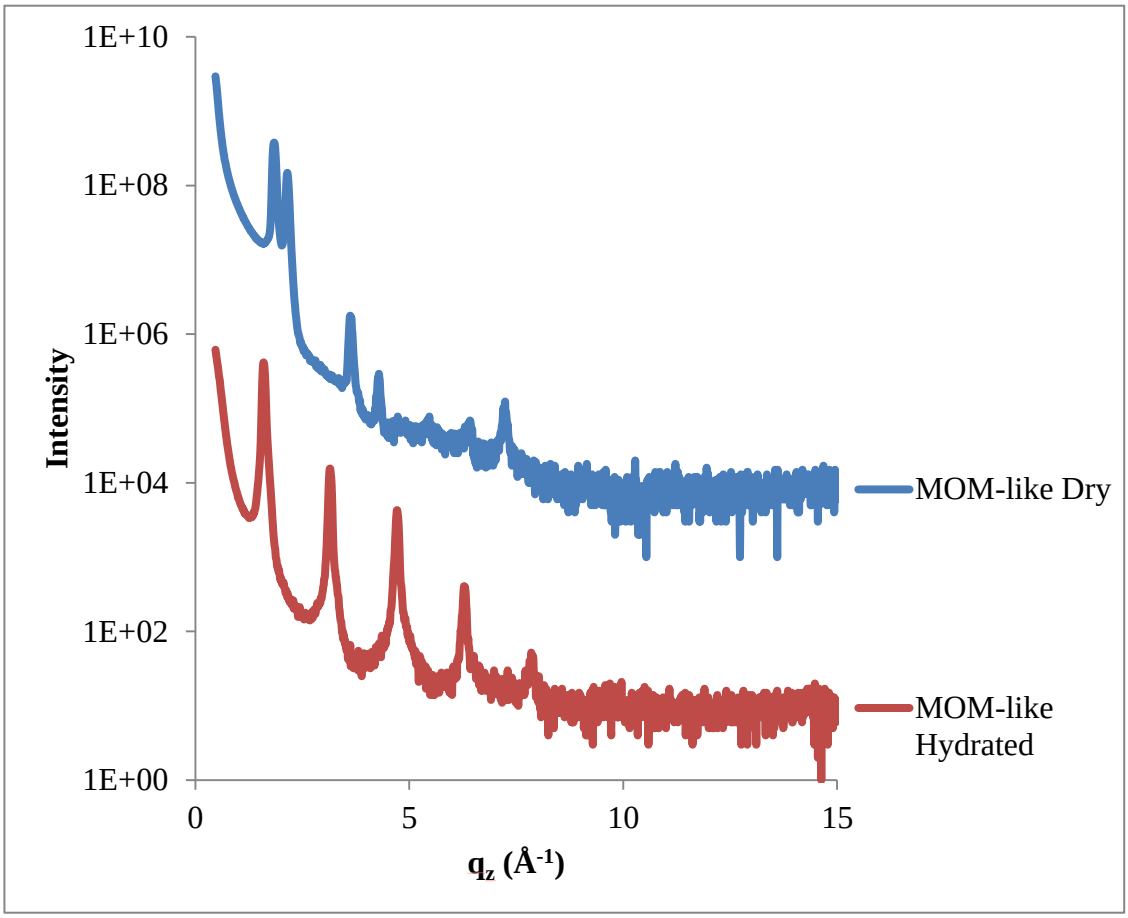

Figure 9: Standard Sample Preparation Protocol Effects on MOM-like Samples. The MOM-like Dry curve has been raised above the hydrated curve for and easy comparison of the two. Use of the standard protocol results in samples that contain two distinct structures within the sample along with some intrinsic disorder, as is seen via the missing higher order peaks. Typically, the number of peaks decreases with increased hydration due to increased fluctuations at lower length scales.

Substrate	Acid (3:1)			Transfer Cleaning (alternate)		APTES (1%)		Transfer Cleaning	
	Temperature	Time	Tilt & Speed	Water (3x)	Ethanol (3x)	Time	Tilt & Speed	Methanol (3x)	Noble Gas Dry
1 cm^2 Silicon	25°C	~30 min.	1 & 15	X	X	~12 hours	1 & 15	X	

Anneal			Transfer Cleaning (alternate)		Deposition						
Vacuum	Temp.	Time	Methanol (3x)	Noble Gas Dry	Concentration	Volume	Temperature	Time	Tilt & Speed	Petri Dish	Noble Gas
X	115°C	3 hrs.	X	X	15 mg/mL	50 µL	40°C	~30 min.	1 & 15	X	

Anneal			Hydration (K_2SO_4)				Storage		Pre-Scan Prep	
Vacuum	Temperature	Time	Temperature		Degassed	Noble Gas	Temperature	Noble Gas	Temperature	Time
			Range	Rate						
X	40°C	~12 hours	25°C-30°C	1°C/hr.			4°C		50°C	3 hours

Table 5: Standard Sample Preparation Protocol. Xs indicate that the step was performed. Substrates were first cleaned in 3:1 H_2SO_4:H_2O_2 acid solution. Substrates were than rinsed and placed in a 1% APTES solution for 12 hours, followed by a rinse and annealing in vacuum overnight. This produced a monolayer of APTES on the substrate. Substrates were then rinsed and lipid solutions were deposited at 50°C and allowed to evaporate in a petri dish in argon gas filled environment. Samples were than annealed for 12 hours and slowly rehydrated to avoid bubbling of the sample. Hydration was conducted under K_2SO_4 supersaturated ultrapure water. Samples were than stored at 4°C in a container filled with argon gas. Prior to use, samples were rehydrated at 50°C to remove any thermal memory from the samples.

4.1) Experimental Procedures Quality Check

Since published methods for multiple bilayer formation (refer to Table 5) did not provide optimal results in the case of the MOM-like lipid composition, we first set out to refine and optimize the experimental protocol for multiple bilayer formation [Tristram-Nagle, 2007; Barrett, 2012]. In order to confirm whether the cause of the variation in reflectivity profiles between identical samples were due to the experimental procedure or the inexperience of the experimenter, several samples identical to those prepared by more experienced users (utilizing the same methodology) were prepared. These samples were much simpler in comparison to the MOM composition, consisting of only one lipid, DMPC, which was kindly provided by Dr. Maikel Rheinstädter's lab. DMPC possess 2 fully saturated 14 carbon tails, has a zwitterionic head group, and has a low transition temperature of 25°C for its liquid phase. Figure 10 compares the reflectivity profiles of several samples (1,2,3, and 4) to a profile provided to us by the Rheinstädter group (referred to as the standard, and prepared by Songbo Zheng). Samples 1 and 2 were prepared roughly one week prior to samples 3 and 4. In addition, the first two were prepared using a chloroform solution for the lipid mixture, while samples 3 and 4, like the standard sample, were prepared in a chloroform and TFE solution. Finally, samples 1 and 3, as the standard, had no hole placed in the petri dish after deposition of the lipid solution onto the substrate, while samples 2 and 4 did. The hole was center on the lid and was roughly 1mm in diameter. This allowed for quicker evaporation from the samples 2 and 4, though this showed no significant alterations to the multilamellar structure of the

samples. In contrast, using a chloroform only solution for the lipid mixtures results in a much more distinctive (separated) peak splitting, as is seen in the reflectivity profiles for samples 1 and 2. Sample 3 was prepared under identical conditions to the standard sample. Despite these small variations, peak positions and relative intensities are similar, including peak splitting and the roughly 0 amplitude 5^{th} peak. A slight shift to lower q_z for samples 1 through 4 is due to slightly lower hydration levels caused by the slightly higher temperature (refer to table 3) of samples 1 through 4. Note the higher resolution of the standard sample due to a longer scan time. Samples show no difference between the use of a hole in the petri dish and no hole. These results are indicative of consistent and good sample preparation, ruling out experimenter inexperience as the cause of inconsistency with the MOM samples.

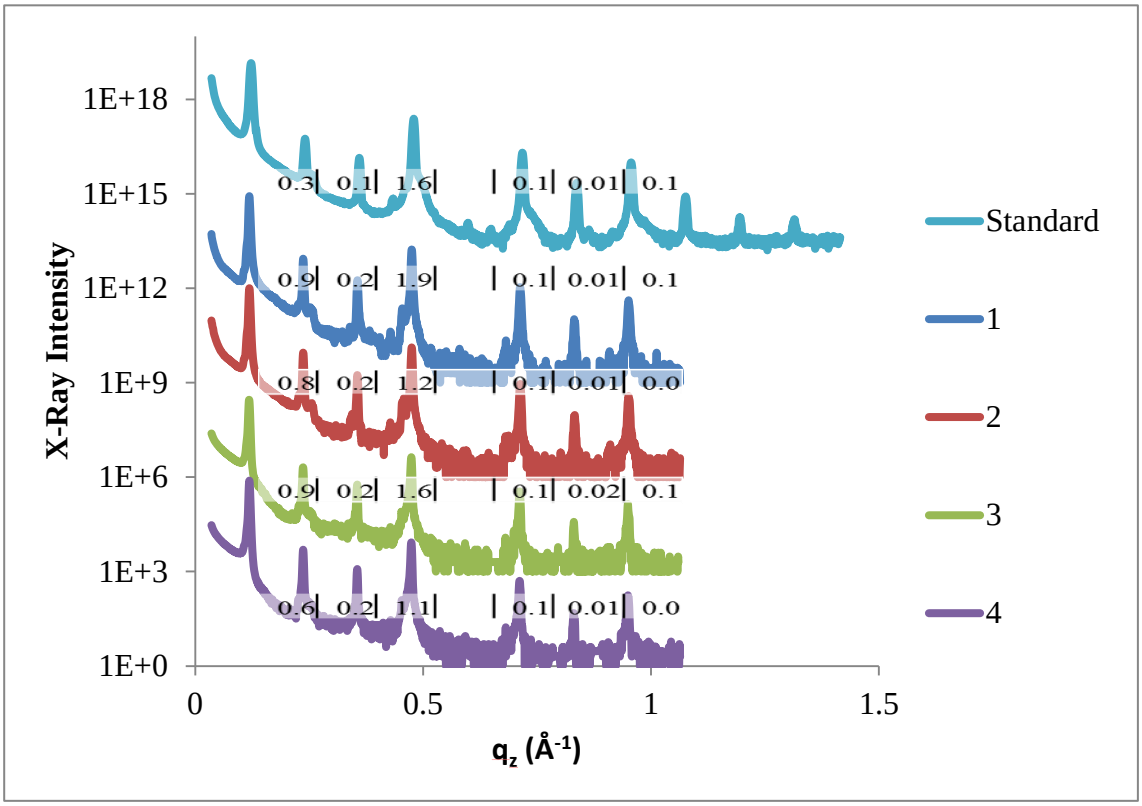

Figure 10: Experimental Technique Comparison. Experimental technique was tested via comparison of DMPC sample production by myself and a more experienced user (labelled standard). Values overlaid on the curves are peak intensities relative to the 1st order peak of the same curve. All scans were completed in the dry state (room humidity). Samples 1 and 2 were prepared using a chloroform solvent; the standard sample and samples 3 and 4 were prepared using a 1:1 ratio of chloroform and TFE. Samples 1 and 3 were also deposited in a completely enclosed petri dish, while samples 2 and 4 had a 2 mm hole drilled in the center for quicker evaporation. Samples 1 and 2 were prepared roughly one week before samples 3 and 4. The Standard sample was scanned at 20°C while samples 1 through 4 were scanned at 22.5°C. The standard data was provided by Matt Barrett from Dr. Maikel Rheinstäder's group.

4.2) APTES Quality Check

In order to elucidate the cause of varied sample quality for the MOM composition, each step of the protocol was tested thoroughly. The first possible cause of sample irregularities was the quality of the APTES layer formed on the silicon wafer and its

effect on lipid deposition. With the acid solution composition kept the same, 3:1 ratio of K_2SO_4 and H_2O_2, the cleaning of the silica wafer was performed at different temperatures (30°C, 40°C and 50°C) for time periods ranging from 5 minutes to 30 minutes. The longer the wafer is in the acid solution, or the higher the temperature, the move vigorous the cleaning of the surface. The rest of the procedure, with the exception of a deposition temperature of 50°C, was carried out according to the standard procedure summarized in Table 5. Figure 11 shows a representative subpopulation of the x-ray reflectivity results taken at room humidity (dry state) and temperature for MOM-like samples prepared with different Acid Bath (AB) temperatures. Samples formed on silicon wafers cleaned at lower temperatures, for up to 30 minutes, resulted in reflectivity profiles with a large number of peaks missing, which are otherwise present in the higher temperature preparation samples as well as in hydrated samples. At higher temperatures, there seems to be a transition at which samples display a large number of peak splitting, indicative of population of substructures within the samples. Samples produced with substrates cleaned at 50°C for a minimum of 15 minutes proved to produce high quality samples consistently.

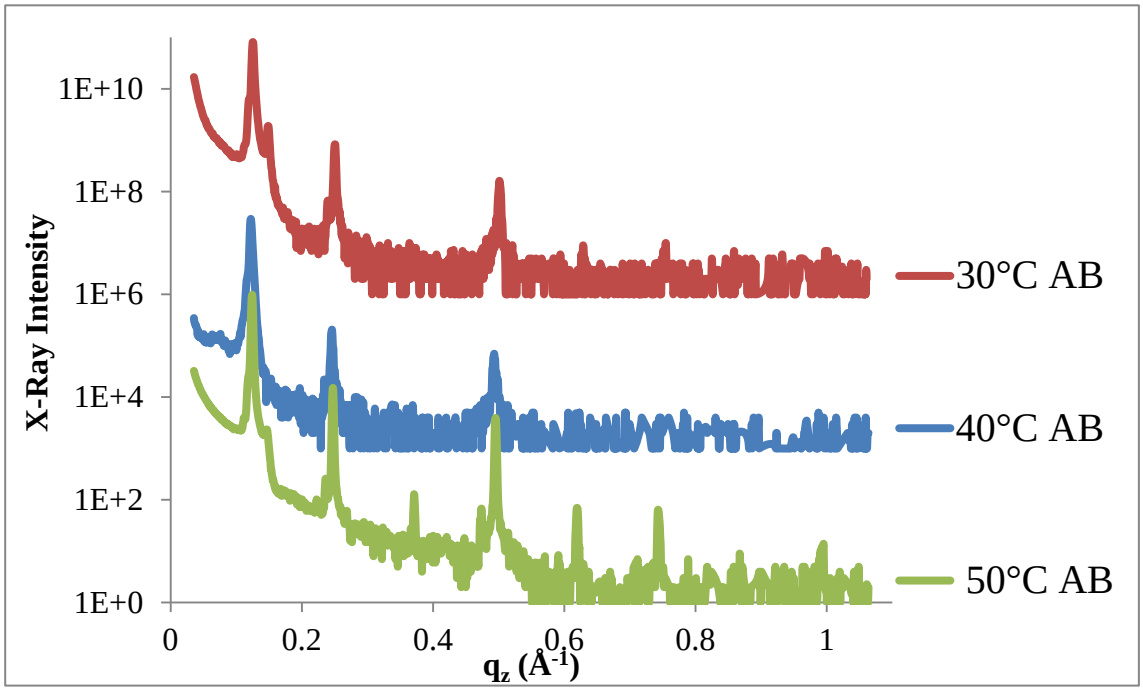

Figure 11: Sample Quality Dependence on Acid Bath (AB) Temperature. Wafers were cleaned in an AB solution of 3:1 H_2SO_4 and H_2O_2 respectively. Cleaned wavers were then placed in an APTES solution; followed by MOM-like lipid solution deposition at 50°C. Low AB temperature for up to 30 minutes results in x-ray reflectivity profiles with relatively few peaks. Increasing AB temperatures to 50°C for a minimum of 15 minutes results in reappearance of higher order peaks.

4.3) Deposition Temperature Quality Check

In addition to acid bath temperature and duration, sample quality was greatly affected by sample deposition temperatures. Mobility of the lipids is essential in order for lipid deposition to form well oriented lipid bilayer stacks. As stated previously, DMPC has a transition temperature of 25°C, and thus formed well-ordered structures above this temperature during deposition. Due to the complex mix and varied transition temperatures of the lipids present in the MOM lipid samples, it was essential to find the correct temperature required to form high quality samples. Figure 12 displays the result

(in their dry state) of depositing samples at several different temperatures ranging from room temperature (RT) up to 50°C. As is clearly evident, the samples prepared at RT display two distinct peaks, indicative of two different size structures present within the sample. As the deposition temperature is increased, the second set of peaks is found to diminish until only one structure is present in the now homogenous sample. A possible explanation for the peak splitting at lower temperatures may be the formation of domains of lipids in the gel phase while the remainder of the sample is in the liquid phase. This is plausible as there are several lipids used to form the samples with varying tail lengths, saturation levels, and transition temperatures. To the best of my knowledge, the transition temperature of the MOM-like mixture has yet to be determined. Figure 12 also shows that the use of a 3-Dimensional rocker (BD) offers little to no improvement in sample quality, however was used for future sample preparations to avoid the possibility of dewetting.

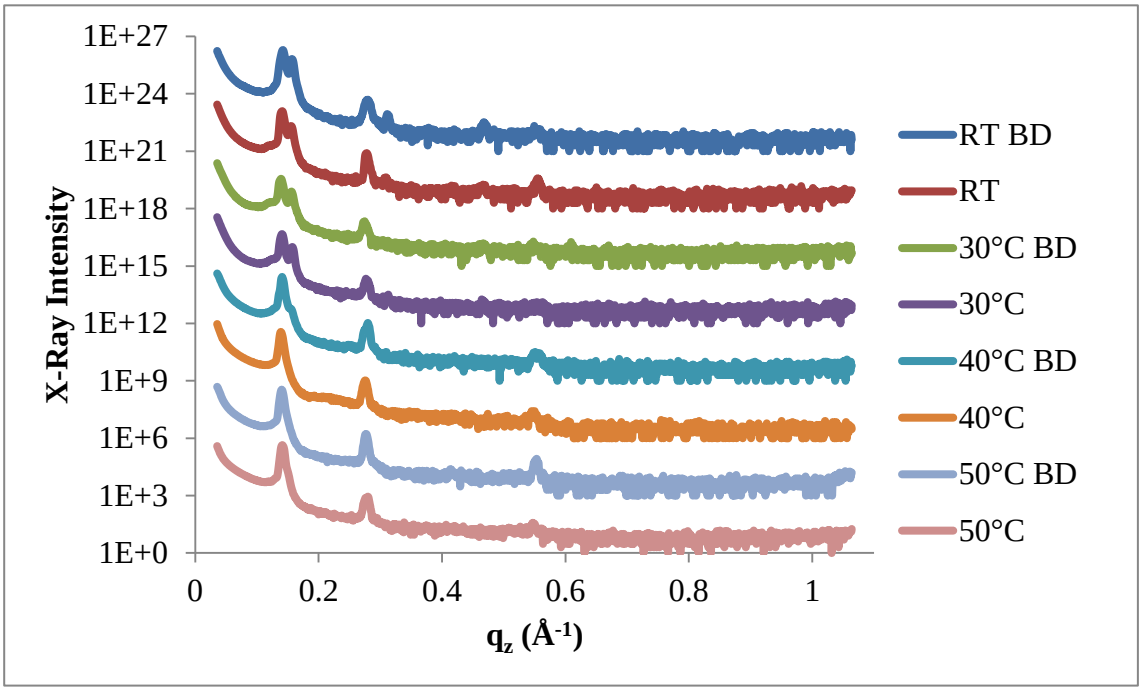

Figure 12: Sample Quality Dependence on Deposition Temperature. Data collected at 22.5°C and room hydration (dry). BD refers to the use of a 3-Dimensional rocker and RT to room temperature. All samples prepared under identical conditions except for the deposition temperature and use of BD as indicated in the legend. Use of BD has little to no effect on sample quality. Depositions at higher temperatures results in improved sample quality as peak splitting reduces; possibly related to transition temperatures of the lipid composition from partly gel and liquid phase to completely liquid phase, allowing for the production of a more homogenous bilayer.

4.4) Substrate Effects on Multilayer Formation

Although the peak splitting seen in the 50°C AB sample (Figure 11) seemed unusual, it was consistent between all samples prepared even under 98% hydration through the use of K_2SO_4. Initially, this posed much concern as to the quality of the sample, and as suggested by Dr. Maikel Rheinstädter, perhaps were due to undesirable repulsive interactions between the substrate and negatively charged lipids within the MOM composition. These interactions may have caused inhomogeneity in lipid composition

from one bilayer to another resulting in the weak peak splitting observed. In order to isolate and test this possibility, a second substrate without any charge, Quartz kindly provided by Dr. Maikel Rheinstädter's group, was tested. Due to the lack of charge, APTES was no longer required in preparation of the samples (refer to Material and Methods). In completing sample preparation, x-ray reflectivity scans were conducted directly after deposition as well as after a hydration phase. All samples showed signs of peak splitting similar to samples prepared on the silicon substrates, suggesting the splitting was an inherent component of the MOM lipid bilayer structure. In addition, samples prepared on quartz substrates did not require samples to be hydrated after the initial deposition as excessive exposure to high levels of humidity resulted in pealing of the sample from the substrate (Figure 13, Quartz 2 – Post Ramping Hydration (Dry Scan)). The molecular disorder caused could however be rectified through hydration of the sample during scanning (Figure 13, Quartz 2 – Post Ramping Hydration (Hydrated Scan)), as was the case with samples prepared using a silicon substrate.

With substrate effects ruled out as a probable cause of peak splitting, and the ability to prepare samples of equal quality repeatedly, the new protocol for the MOM-like samples was completed. Table 6 summarizes the new sample preparation protocol, and highlights the changes made to the standard protocol.

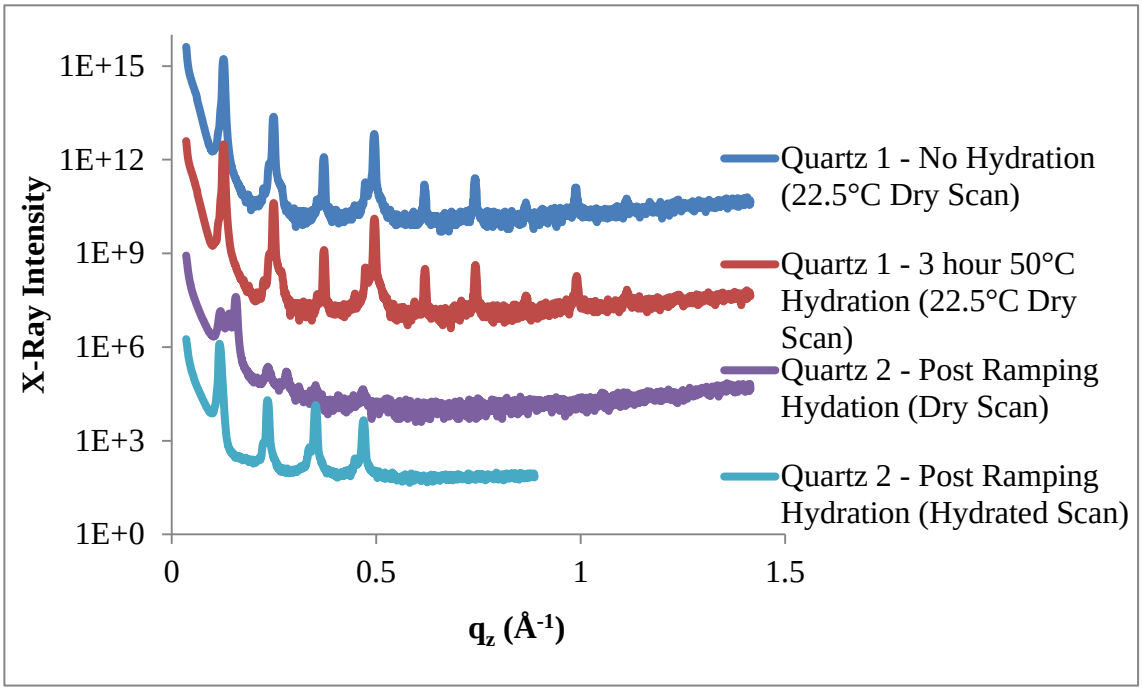

Figure 13: Substrate Effects on Sample Quality. All samples scanned at 22.5°C under room humidity (DRY) conditions unless otherwise specified in the legend. Hydrated scan refers to the use of K_2SO_4 hydration during scanning. Ramping hydration refers to hydration of sample from 20°C to 30°C at 1°C per hour as per the standard protocol. Prevalence of peak splitting from sample to sample prepared in a multitude of protocols arose questions as to possible electrostatic interactions between MOM lipid composition and the substrate. Quartz, a substrate with no surface charge, was used to produce SSLB, resulting in the same peak splitting observed when utilizing quartz. Substrate preparation protocols differed from those used for the silicon substrate, and over exposure to high levels of humidity after deposition of the lipid solution and vacuum drying caused severe disorder within the structure of the bilayers and the sample began to peel off the substrate (purple curve). Under hydration, sample quality was restored, as was observed when using a silica substrate. In addition, scanning the sample at a temperature of 50°C resulted in apparent disappearance of peak splitting, signifying more homogeneous lipid bilayers.

Substrate	Acid (3:1)			Transfer Cleaning (alternate)		APTES (1%)		Transfer Cleaning	
	Temperature	Time	Tilt & Speed	Water (3x)	Ethanol (3x)	Time	Tilt & Speed	Methanol (3x)	Noble Gas Dry
1 cm^2 Silicon	**50°C**	~30 min.	1 & 15	X	X	~12 hours	1 & 15	X	**X**

Anneal			Transfer Cleaning (alternate)		Deposition						
Vacuum	Temp.	Time	Methanol (3x)	Noble Gas Dry	Concentration	Volume	Temperature	Time	Tilt & Speed	Petri Dish	Noble Gas
X	115°C	3 hrs.	X	X	15 mg/mL	50 µL	**50°C**	~30 min.	1 & 15	X	**X**

Anneal			Hydration (K_2SO_4)				Storage		Pre-Scan Prep	
Vacuum	Temperature	Time	Temperature		Degassed	Noble Gas	Temperature	Noble Gas	Temperature	Time
			Range	Rate						
X	40°C	~12 hours	25°C-30°C	1°C/hr.	**X**	**X**	4°C	**X**	50°C	3 hours

Table 6: Modified Sample Preparation Protocol. Final sample preparation protocol modified from the standard protocol featured in table 5. Black values have not changed from that of the standard protocol, red values have been modified from the standard protocol. Xs show the use of the related step. Substrates were first cleaned in 3:1 H_2SO_4:H_2O_2 acid solution. Substrates were than rinsed and placed in a 1% APTES solution for 12 hours, followed by a rinse and annealing in vacuum overnight. This produced a monolayer of APTES on the substrate. Substrates were than rinsed and lipid solutions were deposited at 50°C and allowed to evaporate in petri dish in argon gas filled environment. Samples were than anealed for 12 hours and slowly rehydrated to avoid bubbling of the sample. Hydration was conducted under K_2SO_4 with degassed water and containers filled with argon gas. Samples were than stored at 4°C in a container filled with argon gas. Prior to use, samples were rehydrated at 50°C to remove any thermal memory from the samples.

5) Data Analysis: Phase Determination

Having become confident in the modified sample preparation procedure and its ability to reliably produce high quality samples, the data analysis had to be looked at before final inquisitions into cholesterol content could be started. In contrast to sample preparation quality, which could be tested using the reflectivity profile, testing the experimental environment would require being able to fully analyze data and look at electronic density profiles so as to accurately judge its effects on the sample. As discussed in the Materials and Methods section above, reflectivity profiles were fit using basic Voigt or Gaussian functions over a Fresnel reflectivity background (Figure 14). Utilizing the swelling method, several different salts were used to induce varied levels of hydration to the system, thus resulting in a sequence of d_z values. This data was used to determine the phases ([- - + - -] for a MOM-like sample at 22.5°C and K_2SO_4 hydration) required to Fourier transform the reflectivity data into ED profiles according to the method described in section 3.5.3. Figure 14 shows one such example for a MOM-like sample, with a single reflectivity profile and its fit, the fitting of the data from several hydration levels to the continuous transform, as well as the final resulting ED for the reflectivity profile shown. This data was collected at a temperature of 22.5°C, using NaCl, KCl, and K_2SO_4 salts.

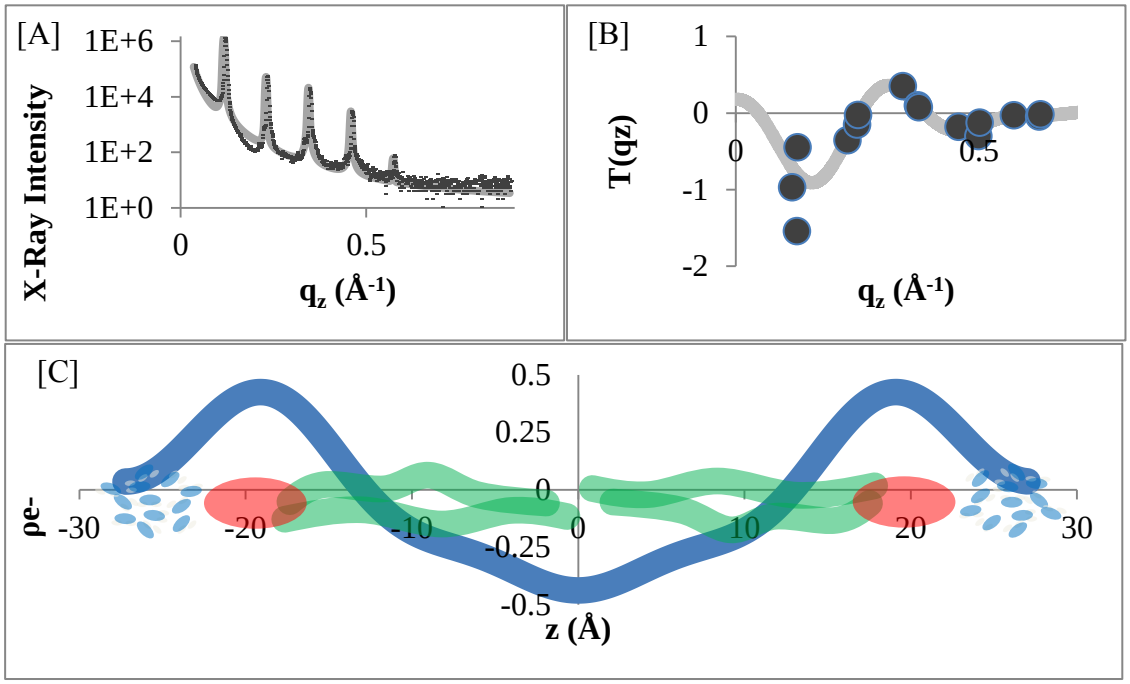

Figure 14: MOM SSLB Data Analysis Outline. [A] Reflectivity data (black markers) and fit (solid grey line) for a MOM SSLB system under K_2SO_4 Hydration at 22.5°C. First four peaks are fit using the Voigt function while the final two are fit using a Gaussian function, all over a q_z^{-4} Fresnel reflection profile and constant background signal. [B] Continuous transform fit utilizing the swelling method resulting in a phase combination of [- - + - -]. Data points represent corrected integrated peak intensities for a MOM sample under NaCl, KCl and K_2SO_4 under 22.5°C hydration conditions. [C] Electron density profile for a MOM under K_2SO_4, 22.5°C hydration. Transparent overlay shows the link between bilayer structure and electron density profile. Red circles, representative of the lipid headgroups contain atoms with higher electron counts, and thus show peaks in the electron density profile. Green lines, represent hydrocarbon tails of lipds, of which one is generally longer than the other and therefore shows a small semi-constant region followed by a small decrease in electron density at the center of the bilayer. In addition, due to hydration of the sample, there is a thin water layer between bilayers, and thus water is present at both ends of the unit cell, represented by the blue and white circles.

6) Temperature Effects on Membrane Structure

Being able to extract the ED profile of samples made it possible to track changes in structure as the environmental conditions were changed. As explained previously, during the refinement of the sample preparation protocol, it became evident that the mix of lipids entering the MOM-like membranes required to be at temperatures of roughly 50°C during deposition. Although these temperatures are irrelevant to physiological functioning of the Bcl-2 family of proteins, it does hint at the possibility of their temperature dependence being linked to structural changes within membranes. Previous reports have noted that lower temperatures result in slower rates of apoptosis [Pryde, 2000]. In order to test this, a MOM-like sample was prepared and 16 minute scans, over an angular range of 20° was conducted over 15 hours, with the temperature ranging from 10°C to 30°C (Figure15). The sample was allotted 1.5 hrs to reach equilibrium under K_2SO_4 hydration, and then the temperature was continuously increased as the 2θ-scans were run, which resulted in a temperature change of roughly 0.4°C per scan. Assuming no change in structure of the sample during this small range of temperature, the slow rate of temperature increase would ensure that the sample stayed in equilibrium throughout the experiment. Interestingly, the MOM-like sample seems to change most dramatically during the initial cooler temperatures below roughly 20°C; after which point the sample is observed to show little change to the unit cell dimensions. In addition, the sample goes through an initial thickening response but then later begins thinning. Utilizing the reflectivity profiles alone would lead to the conclusion that this phenomenon is due to an initial increase in hydration of the sample and the chambers humidity level increases, followed

by possible evaporation of water from the sample as the temperature increases further. Simultaneously, it is also probable to induce changes to the fluidity of the lipids and the level of thermal fluctuations in the sample tails, leading to changes in bilayer thickness. In order to extract the exact combination of these two possible effects, it is essential to calculate the ED profile for the samples. In order to do so, the phases of every sample is required, though due to the amount of time required to do so (each salt requiring roughly three hours to complete), this is an impractical approach. Instead, it is evident that at the 14th scan (roughly 15.3°C) there is a phase inversion of the fourth peak as it passes through an amplitude of 0, but the phases should be the same before and after this point. The phases found for the MOM-like composition at 22.5°C [- - + - -] was utilized for temperatures above 15.3°C, while [- - + + -] was utilized for temperatures above 15.3°C. The ED profiles based of this assumption are shown in Figure 15.

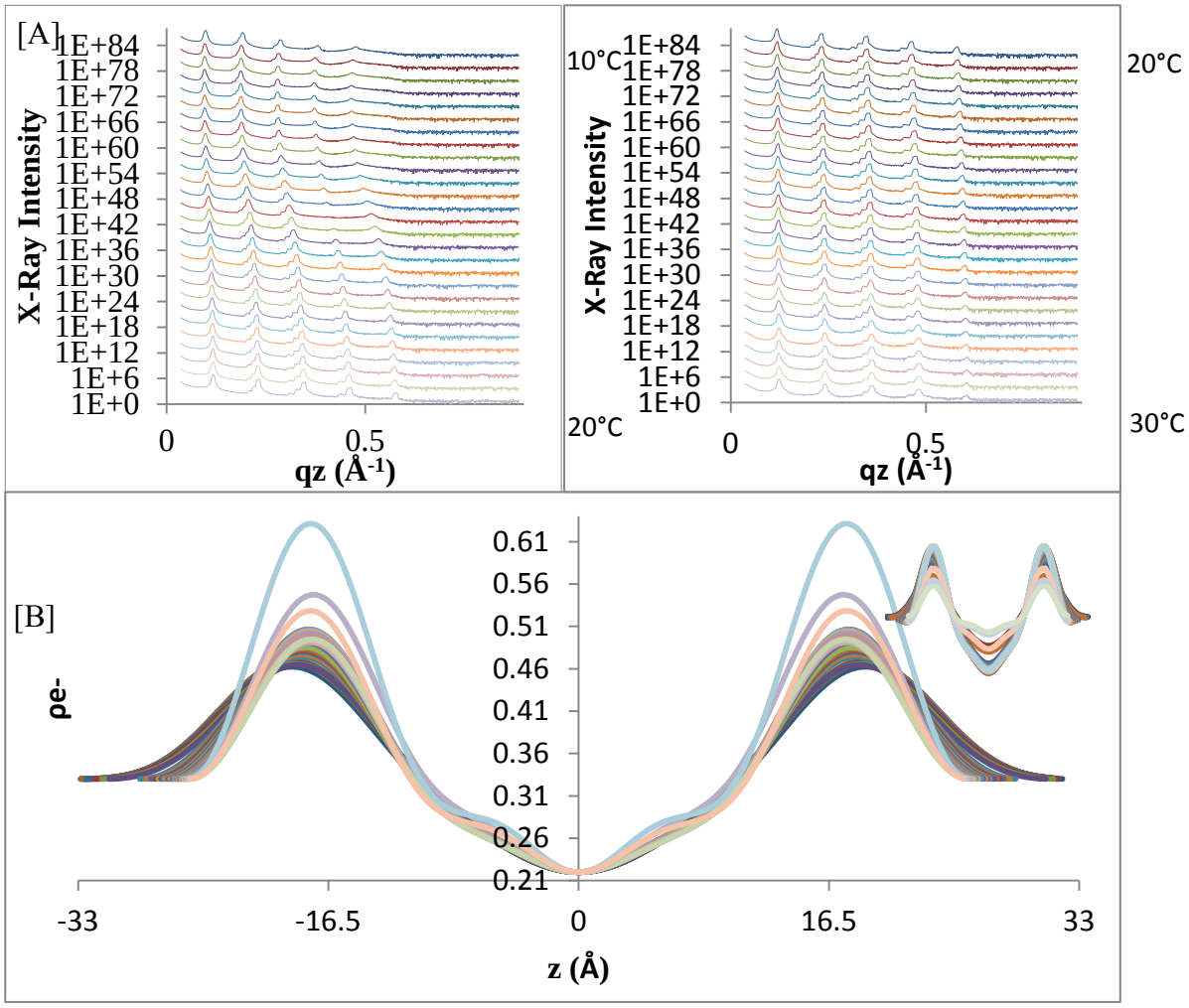

Figure 15: Temperature Effects on MOM-like Bilayers. Scans were completed under K_2SO_4 hydration, with the temperature increasing from 10°C to 30°C over a period of 15 hours continuously. Individual scans lasted approximately 16 minutes, resulting in a temperature variance of roughly 0.4°C per scan, which is negligible with respect to structural changes occurring during the scan. [A] Reflectivity profiles show initial shifts in peak positions being relatively large as compared to higher temperatures (above roughly 17°C). The 4^{th} peak goes through and initially decreases in amplitude until 15.4°C, then proceeds to increase for the remainder of the scans. [B] Electron density profiles were reconstructed utilizing a phase of [- - + - -] above 15.4°C and [- - + + -], as a result of amplitude changes associated with the fourth peak. Inset curves show raw data output of electron densities. Electron densities were normalized utilizing a two point scaling. The water layer between bilayers is expected to have an electron density of 0.33 $e^-/Å^3$, and the center of the bilayer is expected to have the density of a methyl group, 0.22 e-/Å3. Initial temperature increases show a increase of the unit cell as water enters the sample, followed by a decrease (at roughly 13°C) as water evaporates out of the sample. Changes in bilayer thickness are also present as peak shifts, connected to the fluidity of the hydrocarbon tails of the samples.

The ED profiles shed light on what happens during the increase in temperature of the sample. The profiles have been normalized in order to emphasize these changes, though our main interest is related to the thickness of the bilayers, which does not need to be normalized. Normalization was accomplished by scaling of the ED profile based on two known EDs; the water (ED = 0.33 e^-/Å, [Kučerka, 2005]) layer between bilayers found at either extreme as well as the density of a methyl group (ED = 0.22 e^-/Å, [Boer, 1969]) found at the center of the bilayer. These profiles indicate that in addition to a decrease in the water layer between bilayers, there is also a decrease in bilayer thickness. To quantify this, the bilayer thickness, dp-p, (Figure 16 [B]), defined as the peak to peak distance of the ED profile, was subtracted from the total thickness of the unit cell, d, (Figure 16 [A]), resulting in the water layer thickness, dw, (Figure 16 [C]). Upon examination of these curves, it becomes evident that the total thickness (lipid bilayer and water) initially increases slightly, followed by a fast decrease, and then an eventual slower decrease above roughly 18°C. In contrast, the lipid bilayer thickness never seems to change as dramatically and seems to decrease slowly above 15°C. Bilayer thinning with an increase in temperature is expected as an increase in temperature increases the thermal energy of the hydrocarbon chains, increasing the size of their fluctuations parallel to the plane of the membrane and thus decreases their length in the direction perpendicular to the plane of the membrane, thinning the membrane. Water seems to initially enter the sample, increasing the bilayer thickness, followed by evaporation out of the sample as temperatures continue to rise. In addition, changes to water layer thickness range over

12Å while bilayer thickness changes only span a range of 3Å. This point is further emphasized in Figure 16 [D] and [E]. As the temperature is increased above approximately 12°C, the ratio between dp-p/dw increases as a result of the water layer decreasing thickness faster than the bilayer thickness. Moreover, it is observed that both the bilayer thickness and water layer thickness change most dramatically around 15°C, but the amount of change is roughly 4 times larger for the water layer. Thus the majority of thickness changes occurring to the sample upon increasing the temperature are related to the level of hydration present and not to the bilayer itself, though the thickness of the bilayer does decrease slightly.

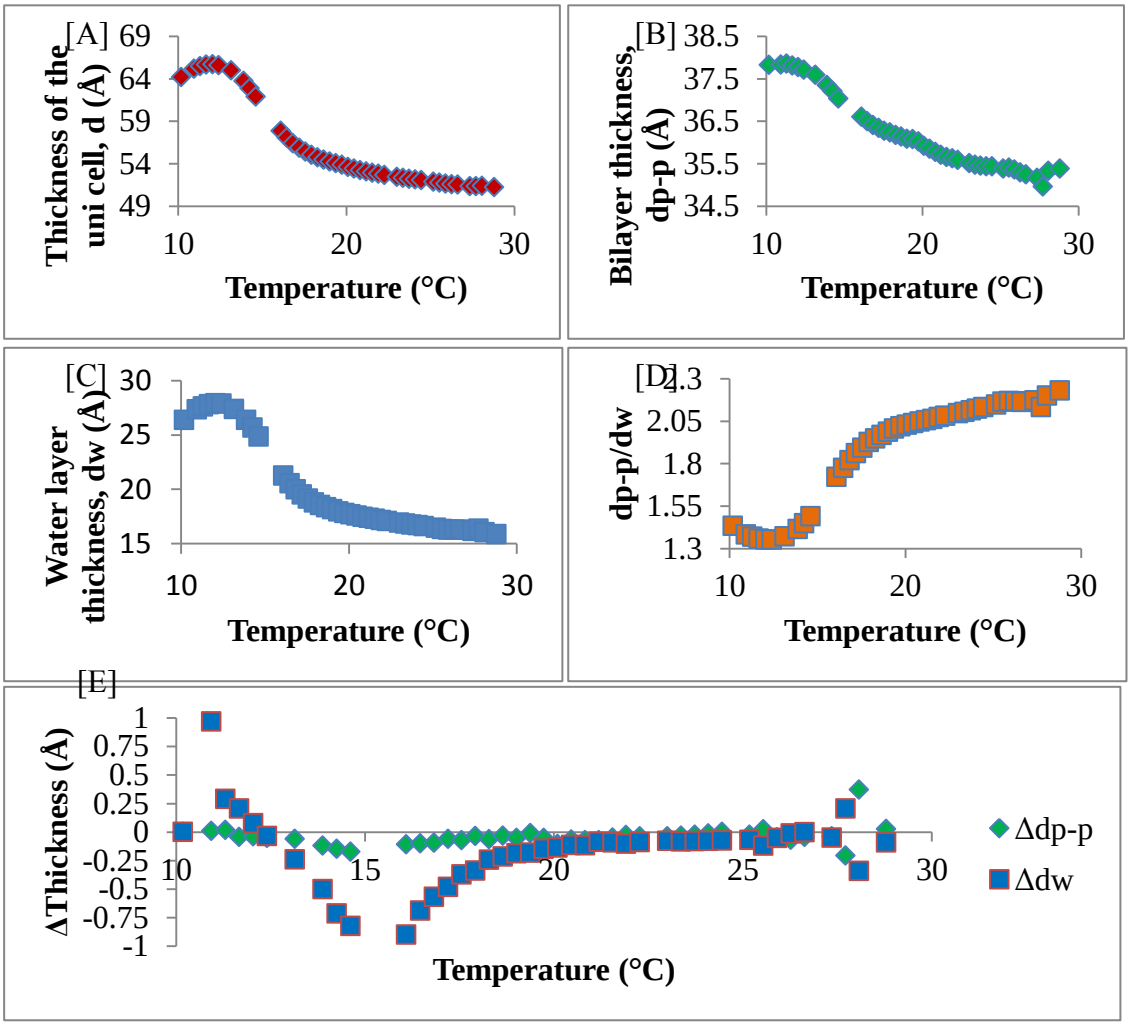

Figure 16: Temperature Related Changes to MOM-like Samples. Scans were completed under K_2SO_4 hydration, with the temperature increasing from 10°C to 30°C over a period of 15 hours continuously. Individual scans lasted approximately 16 minutes, resulting in a temperature variance of roughly 0.4°C per scan. [A] Thickness of a unit cell (bilayer+water) as a function of temperature. [B] Thickness of bilayer (dp-p) defined as the distance between peaks of the electron density profile. [C] Water layer thickness between bilayers defined as the subtraction of (d_z)-(dp-p). [D] Ratio of bilayer to water layer thickness in sample as a function of temperature. [E] Change in thickness between two scans of both the bilayer and water layer.

7) Cholesterol Effects on Membrane Structure

7.1) Cholesterol & Membrane Homogeneity

In order to examine the effects of cholesterol on the MOM-like bilayer and its possible link to the Bcl-2 family of proteins, it was essential to conduct experiments at physiological temperatures and hydration levels, and as such all experiments were conducted at 37°C under K_2SO_4 hydration (about 96.5% relative humidity). In order to avoid condensation of water on to the kapton windows, hot air blowers were used, with the settings summarized in Figure 7. Since temperature scans discussed above indicated little variation in structure and phases above 15.3°C, a [- - + - -] phase combination was used for MOM-like (0% Cholesterol) samples at 37°C. Similar to the temperature study conducted, increasing cholesterol concentration revealed a phase change through the reflectivity profiles for the 5th order peak at as concentrations increased above 25% Cholesterol (Figure 17). Therefore, a phase combination of [- - + - +] was used when analyzing the 30% and 35% cholesterol samples. Ideally, hydration profiles through the use of salts should be collected for all concentration, though instrumental issues prevented such experiments for this thesis. Figure 18 shows the continuous transform data collected for all cholesterol concentrations with the phase combinations discussed above. In addition to the apparent change in phase, it is also worth noting that cholesterol seems to have a stabilizing effect on the bilayers produced as increasing the concentration resulted in a decrease in the peak splitting of the reflectivity profiles. In addition, at larger q values (about 1.05) there is an independent feature (indicated by an arrow), seemingly unrelated to the other bragg peaks due to its large width, found on the 15% and

25% cholesterol samples. These features indicate structures of roughly 6 Å in size and may be an artifact of in-plane structures.

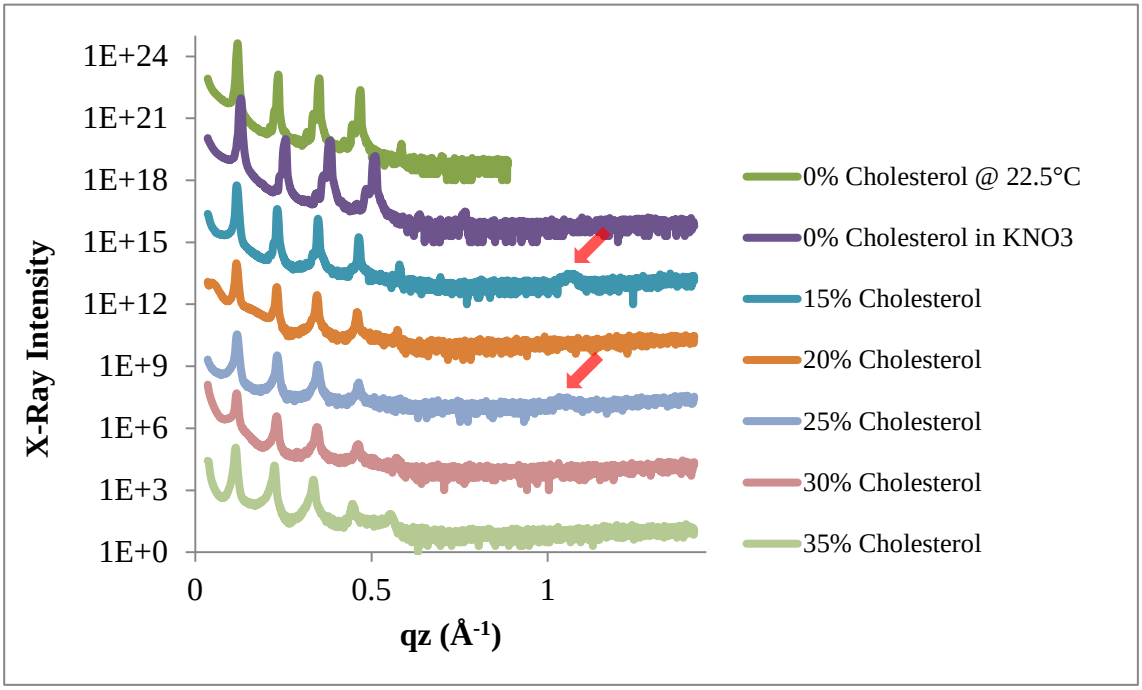

Figure 17: Cholesterol X-Ray Reflectivity Profiles. Reflectivity profiles of SSLB of compositions ranging from 0% cholesterol (MOM composition) to 35% cholesterol content . All samples were scanned at 37°C under K_2SO_4 unless otherwise stated in the legend. Increasing cholesterol content is balanced by decrease the PC content in the composition. 0% samples are under slighly different conditions (either temperature or hydration salt, refer to legend) during scanning and cannot be directly compared to the other samples. Increase cholesterol decreases peak splitting, indicating a more homogenous bilayer structure. Peak 5 decreases in amplitude as cholesterol content is increased to 25%, then begins to increase. Samples of 15% and 25% have broad, low amplitude peaks at about q_z=1.05, relating to a structure of roughly 6 nm.

It should be noted that the two 0% cholesterol concentrations were obtained under slightly different conditions than the other samples. While all cholesterol samples were examined at 37°C and K_2SO_4 hydration, one 0% sample was at 22.5°C, while the other was under KNO_3 hydration; making it impossible to directly compare them to the others as their levels of hydration would be different.

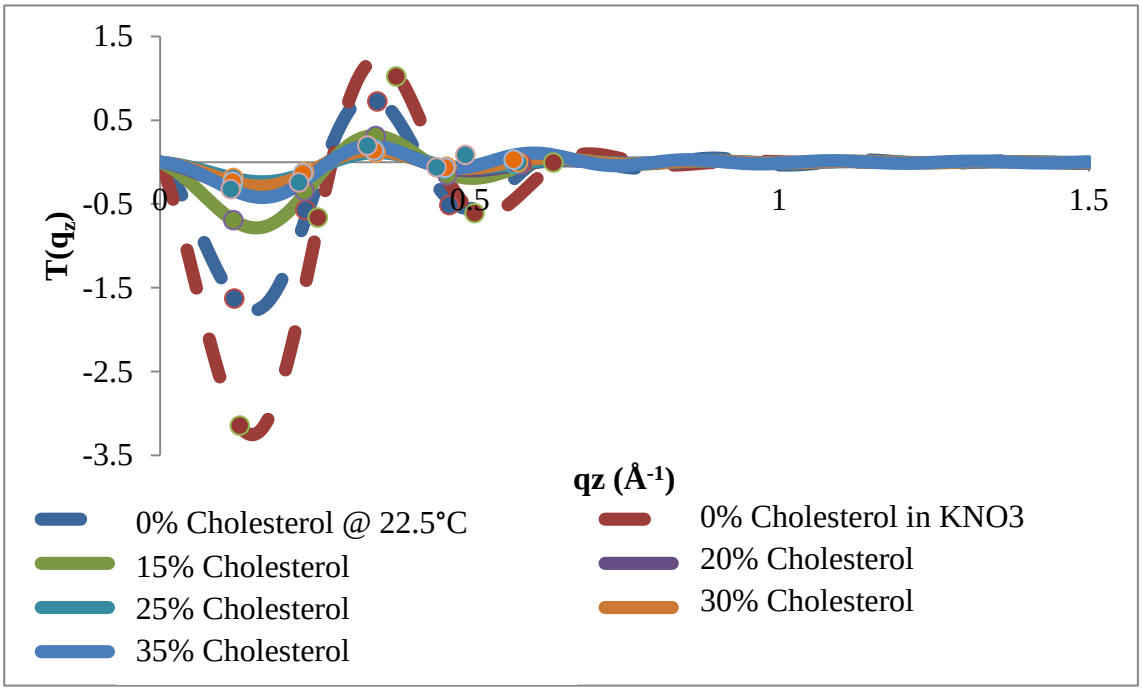

Figure 18: Continuous Transforms for Cholesterol Samples. Data for all samples was collected at 37°C and K_2SO_4 hydration unless otherwise stated in the legend. Phase combination of [- - + - -] was used for concentrations as high as 25% cholesterol after which [- - + - +] was utilized following the 5th peaks amplitude trend (Figure 17). Data points represent corrected integrated peak intensities for cholesterol concentration samples presented in Figure 17.

7.2) Cholesterol and Membrane Structure

In extraction of the ED profiles, it becomes impossible to confidently normalize the results as was done previously. This is due to the apparent increase of ED in the core of the membrane above concentrations of 30% cholesterol. Due to previous works (refer to introduction), it is possible for both the ED of the lipid head group region or the core of the bilayer to increase in ED as cholesterol has been observed to preferentially position itself in both orientations, dependent on concentration and lipid composition. Due to the complexity of the MOM lipid composition, it is impossible to differentiate the two and confidently normalize the data. In addition, the increase in ED to the core of the bilayer is suspicious, and the phases used for these profiles should be found explicitly rather than inference through the reflectivity profiles. Figure 19 has both ED profiles in their raw state as calculated through the Fourier transforms, as well as in an arbitrarily scaled version for ease of comparison between the various functions.

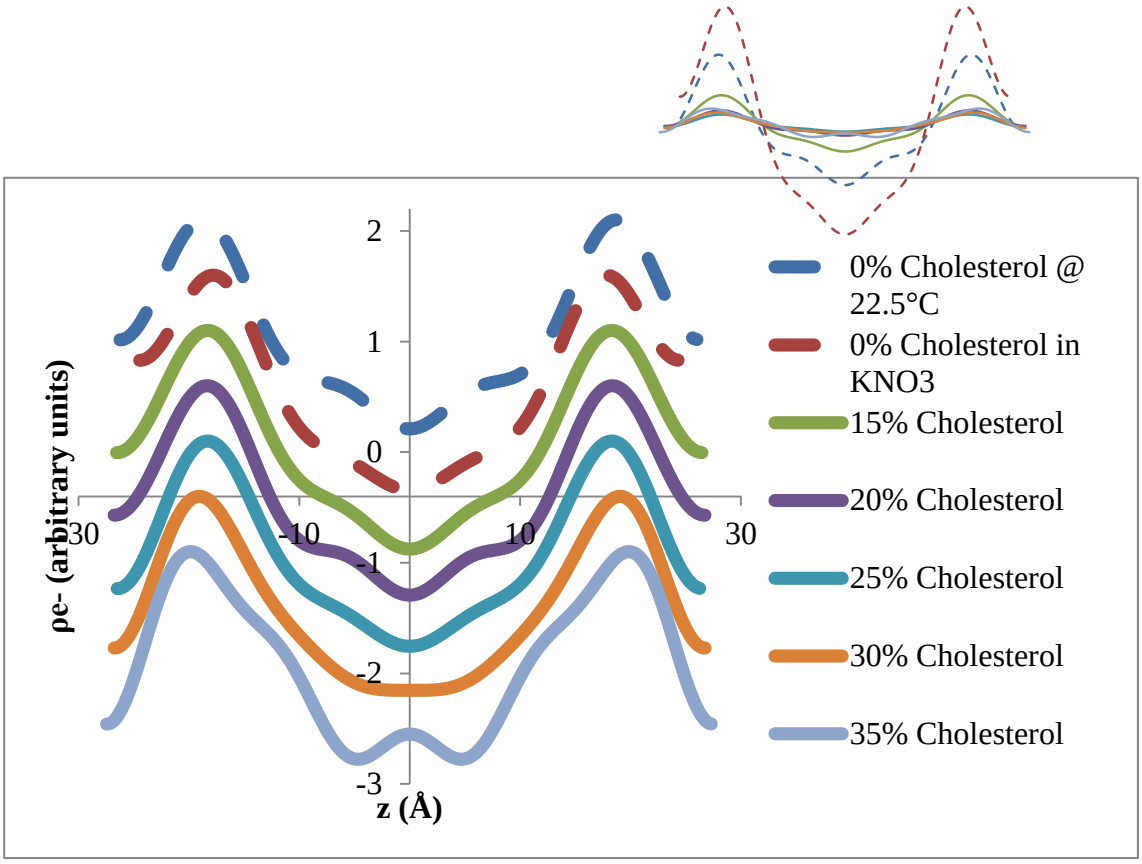

Figure 19: Cholesterol Electron Density Profiles. Data for all samples was collected at 37°C and K_2SO_4 hydration unless otherwise stated in the legend. Electron density was scaled and shifted for ease of comparision between samples. Inset curves show raw data output of electron densities. Both graphs feature relative electron density axis as data was not normalized. Cholesterol causes increase in bilayer thickness as is evident by the increasing distance between peaks in the electron density profiles. Increase cholesterol content also increases density in the center of the membrane above 30%.

Increasing the concentration of cholesterols tends to increase the thickness of the sample, and more importantly the thickness of the bilayer itself (Figure 20, brown curve). This is similar to previous results in which cholesterol is found to thicken bilayers via elongation of the hydrophobic tails by inserting itself into the bilayer, parallel to the lipids [Hung,

2007; Ivankin, 2010]. It is interesting to note that the water layer between bilayers is also seen to decrease slightly over the range of cholesterol concentrations examined.

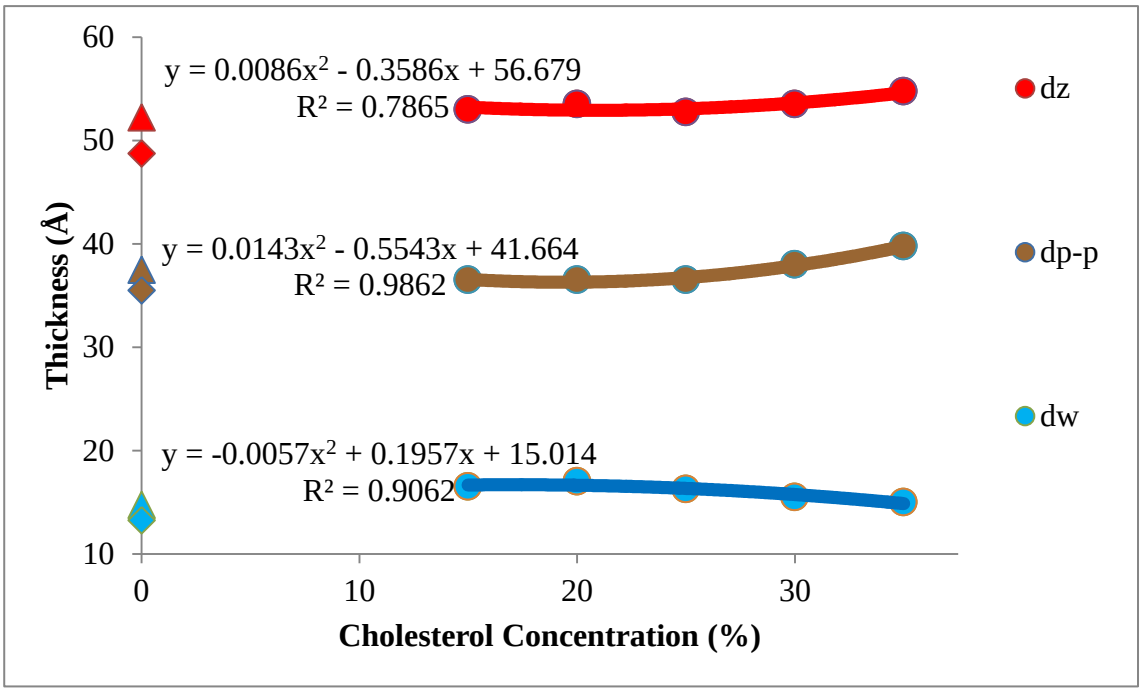

Figure 20: Cholesterol Effects on MOM. All samples are MOM-like compositions with the replacement of PC with cholesterol in the given percentages. The triangular data points are representative of samples hydrated at 22.5°C with the use of K_2SO_4, while diamond data points are representative of samples hydrated at 37°C with the use of KNO_3. Circular data points were hydrated at 37°C under K_2SO_4. D_z is the thickness of the unit cell, which includes both the lipid bilayer and water, dp-p is the peak to peak distance of the electron density profile and is related to the thickness of the bilayer, and finally dw is the water layer thickness in between the bilayers. Increasing Cholesterol Concentration tends to increase bilayer thickness quadratically.

Structural changes caused by the incorporation of cholesterol into the MOM-like samples may shed light on possible explanations towards the inhibition of pore formation by tBid and Bax as observed in previous reports. Taking into consideration that the pore formation of Bax requires partial insertion of its structure (mainly αHs 5,6 and 9), an increase in bilayer thickness may inhibit such insertions as the amphiphilic structure of the αHs no longer matches that of the bilayer. Moreover, Bax pore formation has been noted to decrease bilayer thickness, and bilayer thickening by cholesterol clearly counteracts this. In addition, an increase to the ED of the core of the bilayer may also hinder protein insertion as it may act as a physical barrier that the protein would not be able to pass through. However, both bilayer thickening, and increase in ED of the bilayer core are unlikely explanations for inhibition of Bax pore formation, as an increase of cholesterol content to just 8% already results in a significant decrease in Bax`s pore formation [Shamas-Din, to be published], while significant bilayer thickening and increases in the ED of the core of the bilayer are not observed until roughly 30%. Instead, a more probable explanation may lie in the increased rigidity of the bilayer due to the extension of the lipid`s hydrocarbon chains. Elongation of the lipid tails would result in an increase in the membrane bending energy via a decrease in intrinsic curvature (due to a decrease in their effective area perpendicular to the length of the lipid as a result of chain elongation) of the lipids, which is crucial in the case of lipidic pores.

Conclusion:

Apoptosis is a crucial part of development and growth of both the organism and the cells that it is comprised of. A crucial component of this process, is the Bcl-2 family of proteins and the mitochondria which contains the proapoptotic factors, which once released into the cytosol, result in cell death. The importance of the membrane and its composition, the lipid matrix in particular, has been shown to play a key role in the ability of Bcl-2 proteins, such as tBid and Bax to function. The mitochondrial outer membrane like samples were shown to undergo several changes in its structure based on the temperature and cholesterol content present within them. Lower temperatures have been shown to slow the apoptotic process [Pryde, 2000], and at temperatures below roughly 16°C, the MOM-like membrane is observe to undergo a change in bilayer thickness with a bell shaped profile. Above this temperature, there is a regular decrease in thickness, and is likely due to the increased fluctuations present in the hydrocarbon chains of the phospholipids. In addition to the temperature dependence of protein activity, Bax has been shown to induce membrane thinning, which is assisted by this temperature increase. The addition of cholesterol however has been proven to decrease the pore forming capabilities of Bax, and this may be due to several reasons [Shamas-Din et al., to be published]. This thesis has shown, that with the addition of cholesterol into the membrane, bilayers are observed to increase in thickness. The thickening of the membrane is in direct opposition to the effects of Bax (i.e. membrane thinning), and may

be a possible cause of decreased pore formation. It is important to note however that cholesterol at concentrations as small as 8% has been observed to inhibit this process, while significant changes to bilayer thickness is not observed until concentrations above 25%, diminishing this theory's validity. In addition to membrane thickening, membranes were also observed to have an increased ED in the hydrophobic core above concentrations of 25%. This change in ED of the core of the membrane is also an unlikely candidate for the hindrance of pore formation due to the large quantity of cholesterol required for the effect to be noticeable. Therefore, the inhibition of Bax pore formation is likely due to the increased rigidity of the membrane, as has often been associated with cholesterol. An increase in membrane rigidity would result in an increase in the bending energy of the membrane, which is integral to the formation of lipidic pores, as is the case with Bax. Though this thesis has shed further light on the effects of temperature and cholesterol to the MOM, further studies need to be conducted to verify these findings. Firstly, the ED profiles for samples with cholesterol levels above 25% were reconstructed through an extrapolation of phases based on an observed inversion of peak intensities, in order to confirm this change in phase, a bilayer swelling experiment should be conducted at these concentrations. The increase in ED of the hydrophobic core of the MOM and its link to cholesterol still requires further investigation. This could be accomplished with the use of neutron scattering via phase contrast experiments and selective deuteration. These experiments would also confirm the membrane thickening as was observed in this thesis. In addition to this, in-plain x-ray studies (as well as atomic force microscopy experiments) need to be conducted in order to refine our understanding

of cholesterol within the MOM in the plane of the membrane, specifically to observe the possible formation of domains. In addition, studying a system with both the protein and cholesterol is crucial to solidify the theories extrapolated based on studying the systems individually. Neutron scattering experiments would allow for this via contrast matching through the use of deuterated lipids, proteins, cholesterol and buffer solutions.

References

Adachi, T., (2000). A new method for determining the phase in the X-ray diffraction structure analysis of phosphatidylcholine/alcohol. *Chemistry and Physics of Lipids*, 107, 93-97.

Avanti Polar Lipids, Inc., (2012). *Avanti Polar Lipids, Inc.* Retrieved from http://avantilipids.com/.

Barrett, M.A., Zheng, S., Roshankar, G., Alsop, R.J., Belanger, R.K.R., Huynh, C., Kučerka, N., Rheinstädter, M.C., (2012). Interaction of Aspirin (Acetylsalicylic Acid) with Lipid Membranes. *Public Library of Science ONE*, 7(4), e34357(8).

Basañez, G., Sharpe, J.C., Galanis, J., Brandt, T.B., Hardwick, J.M., Zimmerberg, J., (2002). Bax-type Apoptotic Proteins Porate Pure Lipid Bilayers through a Mechanism Sensitive to Intrinsic Monolayer Curvature. *The Journal of Biological Chemistry*, 277(51), 49360-49365.

Boer, F.P., Turley, J.W., (1969). Structural Studies of Pentacoordinate Silicon. V. Methyl(2,2',3-nitrilodiethoxypropyl)silane. *Journal of the American Chemical Society*, 91(15), 4134-4139.

Buerger, M. J., (1940). The Correction of X-ray Diffraction Intensities for Lorentz and Polarization Factors. *Proceedings of the National Academy of Sciences of the United States of America*, 26(11), 637-642.

Chipuk, J.E., Green, D.R., (2008). How do BCL-2 proteins induce mitochondrial outer membrane permeabilization. *Trends in Cell Biology*, 18(4), 157-164.

Christenson, E., Merlin, S., Saito, M., Schlesinger, P., (2008). Cholesterol Effects on Bax Pore Activation. *Journal Molecular Biology*, 381(5), 1168-1183.

Colbeau, A., Nachbaur, J., Vignais, P.M., (1971). Enzymic Characterization and Lipid Composition of Rat Liver Subcellular Membranes. *Biochimica et Biophysica Acta*, 249, 462-492.

Daillant, J., Gibaud, A., (2009). *X-ray and Neutron Reflectivity Principles and Applications.* Berlin (Heidelberg): Springer Berling Heidelberg.

Danial, N.N., Korsmeyer, S.J., (2004). Cell Death: Critical Control Points. *Cell*, 116, 205-19.

Harris, M.H., Thompson, C.B., (2000). The role of the Bcl-2 family in the regulation of outer mitochondrial membrane permeability. *Cell Death and Differentiation*, 7, 1182-91.

Heit, B., Yeung, T., Grinstein, S., (2011). Changes in mitochondrial surface charge mediate recruitment of signalling molecules during apoptosis. *American Journal Physiol Cell Physiol*, 300, C33-C41.

Huang, H.W., (2006). Molecular mechanism of antimicrobial peptides: The origin of cooperativity. *Biochimica et Biophysica Acta,* 1758(9), 1292-302.

Huang, H.W., Chen, F-Y., Lee, M-T., (2004). Molecular Mechanism of Peptide-Induced Pores in Membranes. *Physical Review Letters*, 92(19), 198304(4).

Hung, W-C., Lee, M-T., Chen, F-Y., Huang, H.W., (2007). The Condensing Effect of Cholesterol in Lipid Bilayers. *Biophysical Journal*, 92, 3960-3967.

Ivankin, A., Kuzmenko, I., Gidalevitz, D., (2010). Cholesterol-Phospholipid Interactions: New Insigts from Surface X-Ray Scattering Data. *Physical Review Letters,* 104, 108101(4).

King, G.I., Worthington, C.R., (1971). Analytic Continuation as a Method of Phase Determination. *Physics Letters,* 35A(4), 259-260.

Kučerka, N., Liu, Y., Chu, N., Petrache, H.I., Tristram-Nagle, S., Nagle, J.F., (2005). Structure of Fully Hydrated Fluid Phase DMPC and DLPC Lipid Bilayers Using X-Ray Scattering from Oriented Multilamellar Arrays and from Unilamellar Vesicles. *Biophysical Journal*, 88, 2626-2637.

Kučerka, N., Marquardt, D., Harroun, T.A., Nieh, M-P., Wassall, S.R., Katsaras, J., (2009). The Functional Significance of Lipid Diversity: Orientation of Cholesterol in Bilayers Is Determined by Lipid Species. *Journal American Chemical Society,* 131, 16358-16359.

Kuwana, T., Mackey, M.R., Perkins, G., Ellisman, H., Latterich, M., Schneiter, R., Green, D.R., Newmeyer, D.D., (2002). Bid, Bax and Lipids Cooperate to Form Supramolecular Openings in the Outer Mitochondrial Membrane. *Cell,* 111, 331-342.

Lange, Y., Ramos, B.V., (1983). Analysis of the Distribution of Cholesterol in the Intact Cell. *The Journal of Biological Chemistry,* 258(24), 15130-15134.

Leber, B., Lin, J., Andrews, D.W., (2007). Embedded together: The life and death consequences of interaction of the Bcl-2 family with membranes. *Apoptosis,* 12, 897-911.

Leber, B., Lin, J., Andrews, D.W., (2010). Still embedded together binding to membranes regulates Bcl-2 protein interactions. *Oncogene*, 29, 5221-5230.

Lee, M-T., Hung, W-C., Chen, F-Y., Huang, H.W., (2008). Mechanism and kinetics of pore formation in membranes by water-soluble amphipathic peptides. *PNAS*, 105(13), 5087-5092.

Liu, J., Durrant, D., Yang, H-S., He, Y., Whitby, F.G., Myszka, D.G., Lee, R.M., (2005). The interaction between tBid and cardiolipin or monolysocardiolipin. *Biochemical and Biophysical Research Communication*, 330, 865-870.

Luken-Ardjomande, S., Montessuit, S., Martinou, J-C., (2008)*. Bax activation and stress-induced apoptosis delayed by the accumulation of cholesterol in mitochondrial membranes. *Cell Death and Differentiation*, 15, 484-493.

Luken-Ardjomande, S., Montessuit, S., Martinou, J-C., (2008). Contributions to Bax insertion and oligomerization of lipids of the mitochondrial outer membrane. *Cell Death and Differentiation*, 15, 929-937.

Martínez-Abundis, E., Correa, F., Pavón, N., Zazueta, C., (2009). Bax distribution into mitochondrial detergent-resistant microdomains is related to ceramide and cholesterol content in postischemic hearts. *Federation of European Biochemical Societies Journal*, 276, 5579-5588.

Martinou, J-C., Youle, R., (2011). Mitochondria in Apoptosis: Bcl-2 Family Members and Mitochondrial Dynamics. *Developmental Cell*, 21, 92-101.

Petros, A.M., Olejniczak, E.T., Fesik, S.W., (2004). Structural biology of the Bcl-2 family of proteins. *Biochimica et Biophysica Acta*, 83-94.

Pryde, J.G., Walker, A., Rossi, A.G., Hannah, S., Haslett, C., (2000). Temperature-dependent Arrest of Neutrophil Apoptosis. *The Journal of Biological Chemistry*, 275(43), 33574-33584.

Satsoura, D., Kučerka, N., Shivakumar, S., Pencer, J., Griffiths, C., Leber, B., Andrews, D. W., Katsaras, J., Fradin, C. (2011). Interaction of the full-length Bax protein with biomimetic mitochondrial liposomes: A small-angle neutron scattering and fluorescence study. *BBA - Biomembranes*, 1818(3), 384-401.

Sorice, M., Manganelli, V., Matarrese, P., Tinari, A., Misasi, R., Malorni, W., Garofalo, T., (2009). Cardiolipin-enriched raft-like microdomains are essential activating platforms for apoptotic signals on mitochondria. *Federation of European Biochemical Societies Letters*, 583, 2447-2450.

Statistics Canada, (2012). *Table 102-0561 Leading causes of death, total population, by age group and sex, Canada.* Retrieved from http://www5.statcan.gc.ca/cansim/a26?lang=eng&retrLang=eng&id=1020561&paSer=&pattern=&stByVal=1&p1=1&p2=37&tabMode=dataTable&csid=.

Tristram-Nagle, S.A., (2007). Preparation of Oriented, Fully Hydrated Lipid Samples for Structure Determination Using X-Ray Scattering. *Methods in Molecular Biology*, 400, 63-75.

Twomey, C., McCarthy, J.V., (2005). Pathways of apoptosis and importance in development. *Journal of cellular and molecular medicine*, 9(2), 345-359.

Yeagle, P.L., (1985). Cholesterol and the cell membrane. *Biochimica et Biophysica Acta*, 822, 267-287.

Yethon, J.A., Epand, R.F., Leber, B., Epand, R.M., Andrews, D.W., (2003). Interaction with a Membrane Surface Triggers a Reversible Conformational Change in Bax Normally Associated with Induction of Apoptosis. *The Journal of Biological Chemistry*, 278(49), 48935-48941.